



**HAL**  
open science

# Self-assembly of amphiphilic amino acid derivatives for biomedical applications

Tengfei Wang, Cécilia Ménard-Moyon, Alberto Bianco

► **To cite this version:**

Tengfei Wang, Cécilia Ménard-Moyon, Alberto Bianco. Self-assembly of amphiphilic amino acid derivatives for biomedical applications. *Chemical Society Reviews*, 2022, 51 (9), pp.3535-3560. 10.1039/D1CS01064F . hal-03811543

**HAL Id: hal-03811543**

**<https://hal.science/hal-03811543>**

Submitted on 11 Oct 2022

**HAL** is a multi-disciplinary open access archive for the deposit and dissemination of scientific research documents, whether they are published or not. The documents may come from teaching and research institutions in France or abroad, or from public or private research centers.

L'archive ouverte pluridisciplinaire **HAL**, est destinée au dépôt et à la diffusion de documents scientifiques de niveau recherche, publiés ou non, émanant des établissements d'enseignement et de recherche français ou étrangers, des laboratoires publics ou privés.

# Self-assembly of amphiphilic amino acid derivatives for biomedical applications

Tengfei Wang, Cécilia Ménard-Moyon,<sup>\*,#</sup> Alberto Bianco<sup>\*,#</sup>

CNRS, Immunology, Immunopathology and Therapeutic Chemistry, UPR3572, University of Strasbourg, ISIS, 67000 Strasbourg, France

Correspondence to: [c.menard@ibmc-cnrs.unistra.fr](mailto:c.menard@ibmc-cnrs.unistra.fr), [a.bianco@ibmc-cnrs.unistra.fr](mailto:a.bianco@ibmc-cnrs.unistra.fr)

<sup>#</sup>These corresponding authors contributed equally to this work.

**Keywords:** bola-amphiphile; cancer therapy; nanostructure; noncovalent interactions; supramolecular chemistry; molecular design; responsiveness

**Abstract:** Amino acids are one of the simplest biomolecules and they play an essential role in many biological processes. They have been extensively used as building blocks for the synthesis of functional nanomaterials, thanks to their self-assembly capacity. In particular, amphiphilic amino acid derivatives can be designed to enrich the diversity of amino acid-based building blocks, endowing them with specific properties and/or promoting self-assembly through hydrophobic interactions, hydrogen bonding, and/or  $\pi$ -stacking. In this review, we focus on the design of various amphiphilic amino acid derivatives able to self-assemble into different types of nanostructures that were exploited for biomedical applications, thanks to their excellent biocompatibility and biodegradability.

## 1. Introduction

The concept of supramolecular chemistry, proposed by J. M. Lehn in 1978, describing the recognition between molecules through noncovalent interactions, has given a new direction to materials science and provided alternative strategies for the design of functional (nano)materials.<sup>1,2</sup> Nanomaterials are materials in which 50% or more of the particles is comprised between 1 and 100 nm size in one or more external dimensions.<sup>3</sup> They have been attracting more and more interest, in particular in biomedicine.<sup>4,5</sup> The development of nanomaterials provided medicine with powerful tools and fostered the emergence of nanomedicine, which is the application of nanotechnology to healthcare.<sup>6</sup> Although some synthetic nanomaterials such as polymers, quantum dots and metal nanoparticles have better stability and higher mechanical strength, their clinical translation might be hampered due to their size/surface property-dependent toxicity, lower biocompatibility and accumulation *in vivo* compared to natural materials.<sup>7,8</sup> Therefore, developing nanomaterials constituted of biomolecules is a promising approach to overcome this problem.<sup>9</sup> Various natural molecules, including proteins, glycans, and nucleic acids, can self-assemble into different nanostructures with a high biocompatibility and biodegradability.<sup>10-13</sup> Peptides and amino acids also display a remarkable self-assembly capacity,<sup>14-16</sup> and the high biocompatibility of their nanostructures allows potential applications in biomedicine, including drug delivery and regenerative medicine.<sup>17-21</sup> Peptides contain a sequence of at least two amino acids coupled by an amide bond. Compared with a single amino acid, peptide sequences give the peptide-based materials more editability. Indeed, by changing the amino acid sequences, peptides with different properties can be easily designed.<sup>22</sup> Moreover, some natural or non-natural peptides, like cell-penetrating peptides,<sup>23</sup> cathelicidin<sup>24</sup> and glutathione (GSH), are already endowed of intrinsic biological activities, and are characterized by well-defined secondary conformations, such as  $\alpha$ -helix or  $\beta$ -sheet, which make them functional without further modifications. However, beside natural peptides, the higher molecular weight of synthetic peptides, compared to single amino acids, makes the control of the self-assembly process more difficult, and the syntheses can be sometimes complicated and can limit their translation into clinical applications. Even though more focus was pointed on the self-assembly of peptides, the study of more simple biomolecules, such as single amino acids, could be closer to the essence of life, when compared to more complex peptides.<sup>25,26</sup> Besides, using single amino acids instead of peptides could avoid complex synthesis and save cost, which is more environmentally and industry friendly. The possibility to functionalize amino acids and the rich diversity of side chains allow diversifying the types of structures obtained by self-assembly, providing an abundant choice for further

developments.<sup>27</sup> In this regard, amphiphilic derivatives designed by conjugating hydrophobic and/or hydrophilic moieties on amino acids can show an improved self-assembly capacity *via* multiple noncovalent intermolecular interactions.<sup>28</sup> While the hydrophilic groups of the amphiphilic amino acid derivatives, like amines and carboxylic acids, are mainly engaged in hydrogen bonds (H-bonds) and electrostatic interactions, the hydrophobic parts can exert hydrophobic forces or  $\pi$ -stacking in the case of aromatic moieties.<sup>29-31</sup> Moreover, the self-assembly process can be controlled and regulated by the hydrophilic-lipophilic balance (HLB).<sup>32</sup> In addition, to modulate the self-assembly of the amino acids, their modification with hydrophilic and/or hydrophobic moieties can bring novel properties that can be exploited for fluorescence imaging and targeted drug delivery, for instance, thus enriching the functions of nanomaterials and their applications.<sup>33-35</sup> All these studies allow realizing the importance of the rational design of amphiphilic molecules and the influence of the hydrophobic/hydrophilic moieties on the self-assembly process as well as the material functions. In spite of their significant advantages and promising prospects, there is only a very limited number of reviews on the biomedical applications of supramolecular structures made of single amphiphilic amino acids.<sup>36</sup> In this review, we provide an overview of the research about the diversity and potential of amphiphilic amino acid derivatives to self-assemble into nanostructures with applications in the biomedical field. We focus on the studies reported in the last ten years (after 2010). The different amino acid derivatives are classified based on a precise molecular design: (i) the conjugation of hydrophobic moieties to hydrophilic amino acids, (ii) the derivatization of hydrophobic amino acids with hydrophilic groups, (iii) the derivatization of amino acids with both hydrophilic and hydrophobic chains, and (iv) the assembly of symmetric and bola-amphiphilic structures. We aim to give insights into the design of amphiphilic amino acid derivatives and help understanding the relationship between the molecular design, the self-assembly process, the structure of the self-assembled nanomaterials and their properties and biomedical applications, which is essential for the development of advanced functional materials.

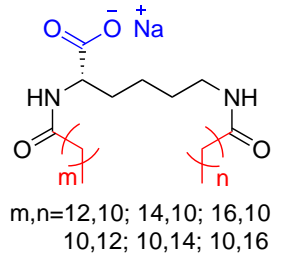
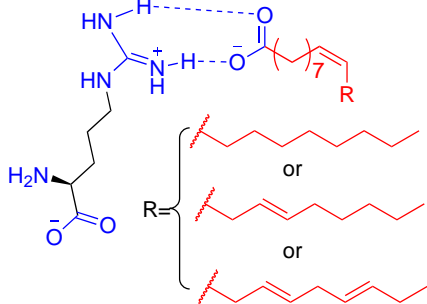
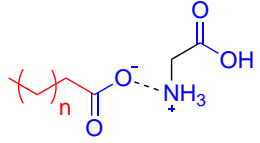
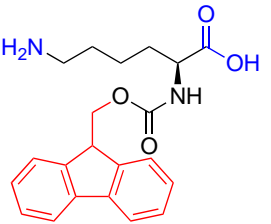
## **2. Amino acid derivatization with hydrophobic moieties**

Amino acids featuring ionizable amino and carboxyl groups are commonly used as hydrophilic parts when designing amphiphilic derivatives. Various hydrophobic moieties, including alkyl chains, the fluorenylmethoxycarbonyl (Fmoc) protecting group, fullerenes, aromatic groups, cyclo- and heterocyclic alkanes were conjugated to the amine and/or carboxylic acid. The hydrophobic moieties can contribute not only to the self-assembly process, but they can also

bring new features to the amino acids. The structures of the amphiphilic molecules described in this section, the type of self-assembled structures and their biomedical applications are summarized in Table 1.

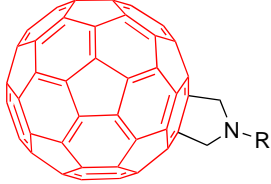
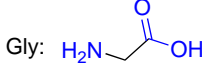
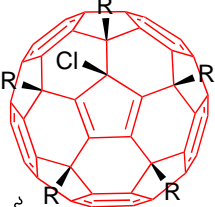
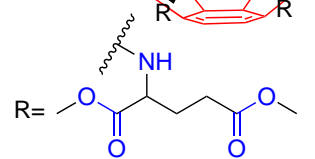
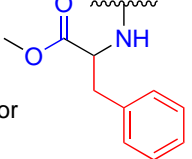
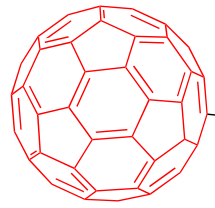
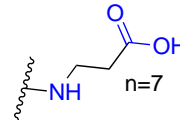
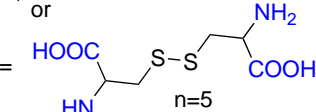
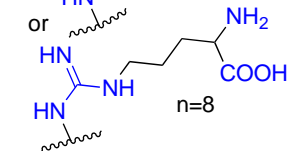
Table 1. Amphiphilic amino acid derivatives modified by hydrophobic moieties.

Entry	Amino acids	Molecular structures	Self-assembled structures	Applications	Ref.
The main hydrophilic and hydrophobic moieties are highlighted in blue and red, respectively.					
1	Trp Tyr		Fibers (hydrogels)	Antibacterial	37
2	Ala Ser		Spherical micelles	Antibacterial	38
3	Gly		Microfibers (organogels)	pH-sensitive release of vitamin B <sub>12</sub>	39
4	Lys		Nanoparticles (co-assembly with chitosan)	pH-sensitive release of methotrexate and anticancer activity <i>in vitro</i>	40

5	Lys	 <p>m,n=12,10; 14,10; 16,10 10,12; 10,14; 10,16</p>	Tubules and ribbons (hydrogels)	pH-sensitive release of lysozyme (antimicrobial protein)	42
6	Arg		Lamellar structures or spherical vesicles	Sustained release of calcein	43
7	Gly	 <p>n=1, 2, 3, 4</p>	Spherical vesicles or micelles	None	44
8	Lys		Nanoparticles (co-assembly with Ce6)	PDT for cancer treatment <i>in vivo</i>	45

9	Leu		Nanoparticles (co-assembly with Ce6 and Mn <sup>2+</sup> ions)	MRI and PDT for cancer treatment <i>in vivo</i>	47
10	His		Nanoparticles (co-assembly with Zn <sup>2+</sup> ions)	PDT for cancer treatment <i>in vivo</i>	51
10	His		Vesicles (co-assembly with Pc)	Photocatalysis (photo-oxidation)	52
11	His Leu Ala Pro		Nanoparticles and nanofibers (co-assembly with hemin)	Glucose detection	53
11	His Leu Ala Pro		Nanofibers (hydrogels)	Antibacterial properties	58
12	Phe		Nanoparticles transformed into nanotube upon oxidation	Redox control of GPx catalytic activity	59



13	Gly	 <p>1. R = GABA-OtBu  2. R = GABA-GABA-OtBu  3. R = GABA-GABA-GABA-OtBu  4. R = GABA-Gly-OtBu  5. R = GABA-Gly-Gly-OtBu  6. R = GABA-Gly-Gly-Gly-OtBu  7. R = GABA-GABA-Gly-OtBu  8. R = GABA-GABA-Gly-Gly-OtBu  9. R = GABA-GABA-Gly-Gly-Gly-OtBu  10. R = GABA-GABA-GABA-Gly-OtBu  11. R = GABA-GABA-GABA-Gly-Gly-OtBu  12. R = GABA-GABA-GABA-Gly-Gly-Gly-OtBu</p> <p>Gly: </p>	Flower-like, leaf-like, spiral-like, and artichoke-like structures, nanorods, flat nanoparticles and curled nanosheets	Antioxidant activity	65
14	Glu Phe	 <p>R =  or </p>	Bilayer spherical vesicles	Sustained release of 5-fluorouracil, cyclophosphamide, or cisplatin	66
15	$\beta$ -Ala Cystine Arg	 <p>R =  n=7  or   n=5  or   n=8</p>	Vesicles	Antioxidant and ROS scavenging activities	67

16	Lys Glu	<p>Gel 1</p> <p>Gel 2</p> <p>Gel 3</p>	Nanofibers (hydrogels)	2D and 3D patterns for cell culture and differentiation	71
17	Tyr		Nanoparticles	Fluorescence imaging and antioxidant activity	72
18	Lys		Rosette nanotubes (hydrophobic core and hydrophilic surface)	Sustained release of dexamethasone	73

## 2.1. Alkyl chains

Alkyl chains bearing a primary amine, a hydroxyl or a carboxyl group (*i.e.*, fatty acids (FAs)) can be conjugated to amino acids by amidation or esterification. In order to afford enough hydrophobicity contending with the hydrophilicity of the amino acid head groups, long-chain hydrocarbons (> 10 carbon atoms) are generally used as tails. For example, Shome *et al.* synthesized amphiphilic hydrogelators with a tryptophan or a tyrosine head by coupling *n*-hexadecylamine onto the  $\alpha$ -carboxyl group, followed by quaternization of the  $\alpha$ -amine (Table 1, entry 1).<sup>37</sup> The self-assembly of the molecules generated hydrogels with a low minimum gelation concentration, which was indicative of efficient supramolecular interactions. Transmission electron microscopy (TEM) revealed a network of fibers with less than 100 nm width and micrometer length. Thanks to the cationic quaternary amines, the two hydrogels were efficient in killing Gram-positive (G+) bacteria through interactions with the negatively charged peptidoglycan of the bacterial membrane. In order to impart broad spectrum antibacterial properties, Ag nanoparticles (AgNPs) were synthesized *in situ* in the hydrogels without additional reducing agents. The side chains of tryptophan and tyrosine and the positively charged head groups played an important role in facilitating and accelerating the formation of the AgNPs because of their redox activities. These hydrogels could also find potential applications as tissue scaffolds, thanks to their biocompatibility guaranteed by the natural amino acids.<sup>37</sup>

Compared to aromatic amino acids forming fibers, two other amino acids, namely alanine and serine, with shorter side chains (methyl and hydroxymethyl, respectively) can self-assemble into spherical structures when modified with alkyl chains (Fig. 1a and Table 1, entry 2).<sup>38</sup> Indeed, alanine and serine derivatives coupled to *n*-dodecanol by esterification formed polydisperse spherical micelles in water with a small size (2.5 nm for alanine derivatives and 2.6 nm for serine derivatives). Sodium chloride played a key role to control the size of the micelles owing to electrostatic repulsion of the cationic amino groups in a saline environment. Both micelles displayed antibacterial activity against G+ bacteria, and the micelles formed by alanine were more efficient whereas no effect was observed on Gram-negative (G-) bacteria. These studies demonstrate that the amino acid side chains play an important role in guiding self-assembly, by providing different types of noncovalent interactions between the molecules and can make disparity in the material properties.

Besides the carboxyl group, the  $\alpha$ -amine is also widely used as a modification site to connect alkyl chains. In this regard, Roy *et al.* designed an amphiphilic glycine conjugated to

2-dodecylpyridine-5-carboxylic acid by amidation (Table 1, entry 3).<sup>39</sup> The molecule was found to form an organogel in a mixture of water/organic solvents with different ratios (v/v from 1/40 to 1/100), while pure solvents failed to initiate the gelation. Besides, parameters like the solvent, gelator concentration, temperature, and molecular structure also affected the gelation process. Fourier-transform infrared spectroscopy (FTIR) showed that intermolecular H-bonds, involving especially the amide group, facilitated the formation of the fibers and the gelation process. Optical images of the organogels evidenced a network structure in the solvent state, while branched microfibers with ~3.5  $\mu\text{m}$  diameter and more than 100  $\mu\text{m}$  length were observed in the dry state after lyophilization (Fig. 1b). The organogels displayed a viscoelasticity associated to a long-time and good thermal stability. The hydrophobic vitamin B<sub>12</sub> was encapsulated in these organogels. An efficient pH-responsive release was found at pH 2 due to ionization, leading to gel collapse and dissolution.<sup>39</sup>

Amino acids with functional polar side chains, such as lysine, can provide many possibilities for chemical modification. They can be functionalized with two alkyl tails, while the carboxyl group remains the hydrophilic head group. For instance, lysine modified with octanoyl acid at the  $\alpha$  and side chain amino groups, was co-assembled with chitosan, resulting in the formation of nanoparticles with a size of ~180 nm (Table 1, entry 4).<sup>40</sup> They were used as carriers of the anticancer drug methotrexate, displaying pH-sensitive drug release thanks to the different ionic states of the lysine-based amphiphile depending on pH. *In vitro* studies showed that the drug-loaded nanoparticles had a more efficient anticancer effect on cancer cells than the free drug, which may be facilitated by their membrane-lytic properties. Lysine-based amphiphiles and their counterion can exhibit pH-dependent membrane-disruptive features.<sup>40</sup> This property was only triggered in acidic condition, thus avoiding the damage of cytomembranes in the physiological state. By contrast, in the tumor microenvironment or lysosomes, the amphiphiles could increase the solubility of the membrane lipids and induce membrane-lysis through the generation of micelles or *via* the insertion into the membranes.<sup>41</sup> These nanoparticles had good hemocompatibility, indicating the possibility for intravenous administration. In another study, the  $\alpha$  and side chain amines of lysine were modified with alkyl chains of different lengths to generate a series of amphiphilic lysine derivatives (Table 1, entry 5).<sup>42</sup> In basic aqueous solutions (pH 10 to 12), the amphiphiles could self-assemble into various tubular structures (80-2000  $\mu\text{m}$  long) like flattened or hollow tubules, as well as coiled or twisted ribbons, and all these structures formed hydrogels. The length of the alkyl tails and the asymmetry of the amphiphiles affected the self-assembly. For instance, heating the

hydrogels led to a reversible gel-sol transition, and the microstructures changed from tubules to micelles or vesicles (depending on the length of the alkyl chains).<sup>42</sup> These differences mainly resulted from the diversity of the molecular hydrophobicity and H-bonds from the head groups. Depending on the alkyl tails, the hydrogels exhibited different cytotoxicity, some of them showing potential for biomedical applications. The model drug lysozyme, which is an enzyme displaying antimicrobial properties, was loaded in the hydrogels and could be released in pH/temperature-dependent manner. Overall, these studies emphasize that amino acid derivatives not only endow the materials with new functions but also affect the self-assembly process and material properties.<sup>40,42</sup>

Alkyl chains cannot be only attached to amino acids by covalent bonding, but electrostatic interactions between the alkyl chains and the amino acids can also be involved in the self-assembly of amphiphilic compounds. Contrarily to covalent bonds, ionic interactions can be created by simply mixing two compounds without requiring a chemical reaction. By changing pH, the ionic states of the amino acids can be easily modulated. For example, Wang *et al.* mixed arginine and unsaturated fatty acids (UFAs) and investigated their self-assembly behavior in water.<sup>43</sup> The carboxylate of oleic acid, linoleic acid, and linolenic acid was complexed to the guanidinium moiety of arginine through electrostatic interactions (Table 1, entry 6). Phase transition properties were found in the self-assembly process of the three supramolecular amphiphiles when gradually adding the UFAs. The amphiphiles initially formed micelles and turned to bilayer structures when increasing the concentration of UFAs. Different evolutions were observed depending on the UFA structure. Oleic acid-based amphiphiles formed lamellar structures, while those constituted of linoleic acid and linolenic acid formed spherical vesicles. This behavior was ascribed to the difference in the number of C=C bonds in the UFAs. Oleic acid contains only one C=C bond, imparting reduced bending in the self-assembly process and leading to molecular stacking. By contrast, the amphiphiles constituted of linoleic acid and linolenic acid had a higher unsaturated degree and curvature, thus preventing a close packing of the UFAs. FTIR analysis showed that H-bonds, electrostatic and hydrophobic interactions were responsible for the self-assembly of the amphiphiles. Calcein, a hydrophilic fluorescent molecule used as a water-soluble model drug, was loaded in the vesicles, allowing sustained release.<sup>43</sup>

In another study, the self-assembly of supramolecular amphiphiles constituted of glycine and ultrasmall FAs with different chain lengths was investigated.<sup>44</sup> These amphiphiles formed spherical vesicles in water (Fig. 1c and Table 1, entry 7). The self-assembly was modulated by altering the FA/glycine ratio and the FA carbon atom number. Increasing the glycine content

induced the formation of a higher number of vesicles, while increasing the length of the FA led to vesicle size enlargement. Regarding the impact of the FA carbon atom number, mixing butyric acid (C4), valeric acid (C5), and hexanoic acid (C6) with glycine led to the formation of pure vesicles with ~200 nm size, whereas heptanoic acid (C7)/glycine mixture led to the formation of larger micelles (~450 nm) and vesicles (100-300 nm). FTIR spectroscopy confirmed that H-bonds was the dominant interaction. Overall, these results indicate that the use of FAs brings some flexibility in the molecular design, yielding various supramolecular structures that could find potential applications in drug delivery.<sup>43,44</sup>

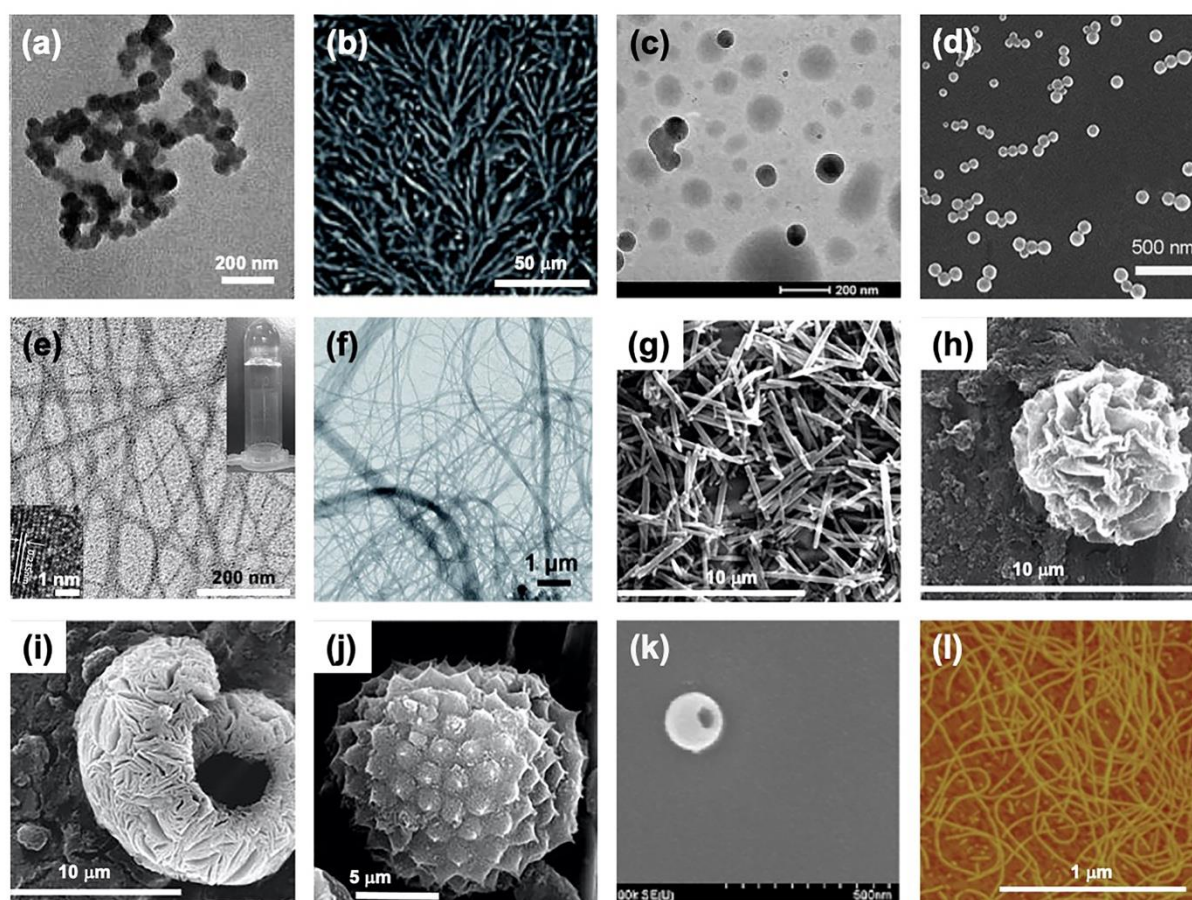


Figure 1. Various nanostructures obtained from the self-assembly of different amphiphilic amino acid derivatives: (a) spherical micelles,<sup>38</sup> (b) microfibers,<sup>39</sup> (c) spherical vesicles,<sup>44</sup> (d) nanoparticles,<sup>45</sup> (e) nanofibers (hydrogel),<sup>58</sup> (f) nanotubes,<sup>59</sup> (g) nanorods,<sup>65</sup> (h) flower-like structures,<sup>65</sup> (i) spiral-like structures,<sup>65</sup> (j) artichoke-like structures,<sup>65</sup> (k) hollow spherical vesicles,<sup>66</sup> (l) rosette nanotubes.<sup>73</sup> Reproduced with permission.<sup>38</sup> Copyright 2014, American Chemical Society. Reproduced with permission.<sup>39</sup> Copyright 2013, the Royal Society of Chemistry. Reproduced with permission.<sup>44</sup> Copyright 2019, Elsevier. Reproduced with permission.<sup>45</sup> Copyright 2016, Wiley. Reproduced with permission.<sup>58</sup> Copyright 2020, Wiley

(Open access). Reproduced with permission.<sup>59</sup> Copyright 2014, the Royal Society of Chemistry. Reproduced with permission.<sup>65</sup> Copyright 2015, Beilstein Institute for the Advancement of Chemical Sciences (Open access). Reproduced with permission.<sup>66</sup> Copyright 2017, Elsevier. Reproduced with permission.<sup>73</sup> Copyright 2011, Dove Medical Press (Open access).

## 2.2. Fmoc-amino acids

The Fmoc group, extensively used to protect amines in solid-phase peptide synthesis, can be also exploited to form supramolecular structures thanks to  $\pi$ - $\pi$  interactions with other aromatic moieties.<sup>29</sup> Amino acids with the  $\alpha$ -amine protected by hydrophobic Fmoc group and with the free hydrophilic carboxylic acid exhibit amphiphilic properties. These derivatives can self-assemble into different structures. As an example, the co-assembly of Fmoc-lysine and chlorin e6 (Ce6), a hydrophobic photosensitizer, led to the formation of homogeneous solid nanoparticles (Fig. 1d and Table 1, entry 8) *via* hydrophobic interactions and  $\pi$ -stacking, together with electrostatic interactions, resulting in high encapsulation efficiency of the drug (more than 80%).<sup>45</sup> The particle size was controlled by tuning the ratio of Fmoc-lysine and Ce6, which can be useful for selecting a suitable size for tumor accumulation through the enhanced permeability and retention effect.<sup>46</sup> For instance, the size could be increased from ~20 to ~200 nm by decreasing the concentration of Ce6. Owing to noncovalent interactions, the nanoparticles displayed multiresponsiveness to pH, surfactants, and lipases, which mimic the microenvironment of lysosomes, enabling a controlled release of Ce6 in the physiological environment. The biodistribution and antitumor capacity of the nanoparticles mediated by photodynamic therapy (PDT) was demonstrated *in vitro* and *in vivo* in tumor-bearing mice.

Fmoc-leucine also demonstrated a co-assembly capacity with Ce6 in the presence of  $Mn^{2+}$  ions, forming solid nanoparticles with ~100 nm size (Table 1, entry 9).<sup>47</sup> In addition to hydrophobic and  $\pi$ - $\pi$  interactions, the coordination bonding with  $Mn^{2+}$  played a key role in the self-assembly process. Indeed,  $Mn^{2+}$  can coordinate with Fmoc-leucine *via* the carboxylate group, and the generated metal-organic coordinate network can encapsulate Ce6 with high loading efficiency (~80%). The nanoparticles were highly stable in a physiological environment, but they were sensitive to GSH. The concentration of GSH is 100-1000-fold higher in cancer cells than in normal cells,<sup>48</sup> and it was suggested that GSH could exhibit a stronger chelation to  $Mn^{2+}$  than Fmoc-leucine, resulting in the nanoparticle disassembly and Ce6 release. Moreover, the chelation between  $Mn^{2+}$  and GSH reduced the GSH level and thus

increased the amount of reactive oxygen species (ROS), making PDT more efficient.<sup>49,50</sup>  $\text{Mn}^{2+}$  ions can be used as contrast agent for magnetic resonance imaging (MRI), allowing tumor localization. Therefore, the chelation of  $\text{Mn}^{2+}$ /GSH also promoted  $\text{Mn}^{2+}$  retention in the tumor cells, allowing real-time monitoring of *in vivo* nanoparticle delivery by MRI (Fig. 2a). The PDT treatment led to an efficient tumor growth inhibition in a breast cancer mouse model.<sup>47</sup>

The strategy of co-assembly mediated by Fmoc-amino acids can be extended to other amino acids, like Fmoc-histidine. Similar to Fmoc-leucine/ $\text{Mn}^{2+}$  system, the coordination between  $\text{Zn}^{2+}$  and the histidine allowed the formation of nanoparticles with ~86 nm diameter (Table 1, entry 10).<sup>51</sup> The imidazole side chain of histidine provides a coordination site for  $\text{Zn}^{2+}$ , in addition to the carboxylate, resulting in a stronger chelation and increased stability. A cationic porphyrin photosensitizer was adsorbed on the negatively charged nanoparticles through a layer-by-layer process exploiting the electrostatic interactions, the coordination with  $\text{Zn}^{2+}$  and the  $\pi$ -stacking, and leading to nanoparticles with a size increased to ~106 nm. The G-rich AS1411 oligonucleotide was subsequently adsorbed on these nanoparticles through electrostatic interactions with porphyrin, forming Fmoc-H/ $\text{Zn}^{2+}$ @porphyrin@AS1411 nanoparticles (~113 nm size). AS1411 aptamer is widely used as targeting molecules for nucleolin overexpressed on tumor cells. The porphyrin/AS1411 complex showed a red-shift of the absorption from 417 nm to the near-infrared region (~700 nm) when compared with the free porphyrin.<sup>51</sup> This feature not only endowed the complex with the capacity of near-infrared-induced PDT, but it also facilitated the cellular internalization of the nanoparticles through nucleolin-mediated endocytosis. Additionally, though AS1411 on the nanoparticles exhibited good stability against nucleases, the nanoparticles showed pH- and GSH-dependent disassembly due to the ionization of the imidazole group of Fmoc-histidine and the competitive binding of GSH to  $\text{Zn}^{2+}$ . The responsiveness of the nanoparticles guaranteed a good biocompatibility in the blood stream and biodegradability to trigger the release of the porphyrin/AS1411 complex. Moreover, the chelation of  $\text{Zn}^{2+}$  with GSH reduced the consumption of  $^1\text{O}_2$  by free GSH and thus increased the effect of PDT. The nanoparticles could accumulate specifically in the tumor of mice and induce a complete suppression of the tumor growth by PDT (Fig. 2b).<sup>51</sup>

Fmoc-histidine can also be co-assembled with phthalocyanine (Pc) to generate nanovesicles with biomimetic catalytic properties *via* multiple noncovalent interactions, including H-bonds,  $\pi$ -stacking, electrostatic and hydrophobic interaction (Table 1, entry 10).<sup>52</sup> The size of the vesicles depended on the molar ratio between Fmoc-histidine and Pc. When the molar ratio



was 1:0.08, the diameter resulted ~142 nm with the membrane thickness of 15 nm. Increasing the amount of Pc increased the size (1:0.25, ~500 nm with 62.5 nm thickness). Pc can be used as a photosensitizer with photooxidase activity, but its application is limited by its hydrophobic properties, resulting in aggregation in aqueous media and fluorescence quenching. This issue was circumvented by the co-assembly with Fmoc-histidine, leading to water-stable vesicles. The distribution of Pc inserted into the membrane of the vesicles could be tuned, avoiding aggregation of the molecule and preserving its fluorescence properties. As a result, the catalytic efficiency of Pc was enhanced and the co-assembled nanovesicles were used as mimetic of photooxidase to catalyze the oxidation of dopamine.<sup>52</sup>

Another functional molecule, hemin, was also co-assembled with Fmoc-histidine, resulting in the formation of nanoparticles and nanofibers (Table 1, entry 10).<sup>53</sup> Similarly, the molar ratio of Fmoc-histidine and hemin could influence the type of self-assembled structures, as increasing the amount of the protected amino acid allowed obtaining large nanoparticles. For example, a ratio of 2:1, 4:1, and 6:1 was used to form nanoparticles with a size of ~50, ~85, and ~120 nm, respectively. By contrast, a ratio of 12:1 led to the formation of nanofibers. The nanoparticles exhibited a peroxidase activity higher than free hemin and the nanofibers, indicating that the catalytic activity could be influenced by the environment of hemin and the self-assembled structure. Moreover, Fmoc-histidine also contributed to enhance the catalytic activity by stabilizing the substrates and providing push-pull electron effect during the catalytic process. The nanoparticles showed good repeatability and structural stability and were used to detect glucose. These studies show that Fmoc-amino acids can be used for co-assembling with hydrophobic functional molecules to achieve high molecular loading efficiency due to  $\pi$ -stacking and hydrophobic interactions provided by the Fmoc group.<sup>45,47,51-53</sup> In this case, an adjustability of the self-assembled structures can be achieved by simply changing the ratio of the Fmoc-amino acid and the functional molecule, with a consequent control on the performance of the nanostructures.

Besides the formation of nanoparticles, Fmoc-amino acids can also form fibrous networks leading to hydrogels.<sup>54-56</sup> Recent studies revealed important details on the self-assembly process of Fmoc-amino acids indicating that the formation of metastable nanoparticles can occur in the early stage of the self-assembly and be transformed into nanofibers prolonging the process.<sup>57</sup> For instance, Fmoc-proline, Fmoc-histidine, Fmoc-alanine, and Fmoc-leucine can form nanofibers (~20 nm width and micron scale in length) and hydrogels driven by H-bonds, hydrophobic interactions and  $\pi$ -stacking (Fig. 1e and Table 1, entry 11).<sup>58</sup> In the presence of

Ag<sup>+</sup> ions, well-dispersed ultrasmall AgNPs (less than 6 nm size) were generated all along the hydrogel fibers by *in situ* reduction. The tris(hydroxymethyl)aminomethane (Tris)-HNO<sub>3</sub> buffer used to dissolve the Fmoc-amino acids and form the hydrogels, also served as a reductant for *in situ* mineralization of the Ag<sup>+</sup> ions, thanks to the hydroxyl groups of Tris. The coordination interaction between the Ag<sup>+</sup> ions and the Fmoc-amino acids allowed the AgNPs to attach uniformly onto the hydrogel network. Moreover, the hydrogels displayed tunable mechanical properties by changing the Ag<sup>+</sup> concentration.<sup>58</sup> Besides, the balance of different intermolecular interactions is essential to maintain the hydrogel structure. For example, excessive hydrophobic interactions enhanced by the coordination of Ag<sup>+</sup>/Fmoc-amino acid may alter the balance of intermolecular force, leading to precipitation rather than hydrogels. The hydrogels showed good biocompatibility and biodegradability with the ability of sustained Ag<sup>+</sup> release. These hydrogels exhibited a high and broad-spectrum antibacterial activity against G<sup>+</sup> and G<sup>-</sup> bacteria through bacterial membrane fusion, clumping, and decomposition. They showed some potential as injectable antimicrobial dressings for wound healing in a wound mouse model after infection with *Staphylococcus aureus*. In addition to the AgNPs, the Fmoc-amino acids may also contribute to the antibacterial process by binding and breaking the bacterial membrane through hydrophobic interactions.<sup>58</sup>

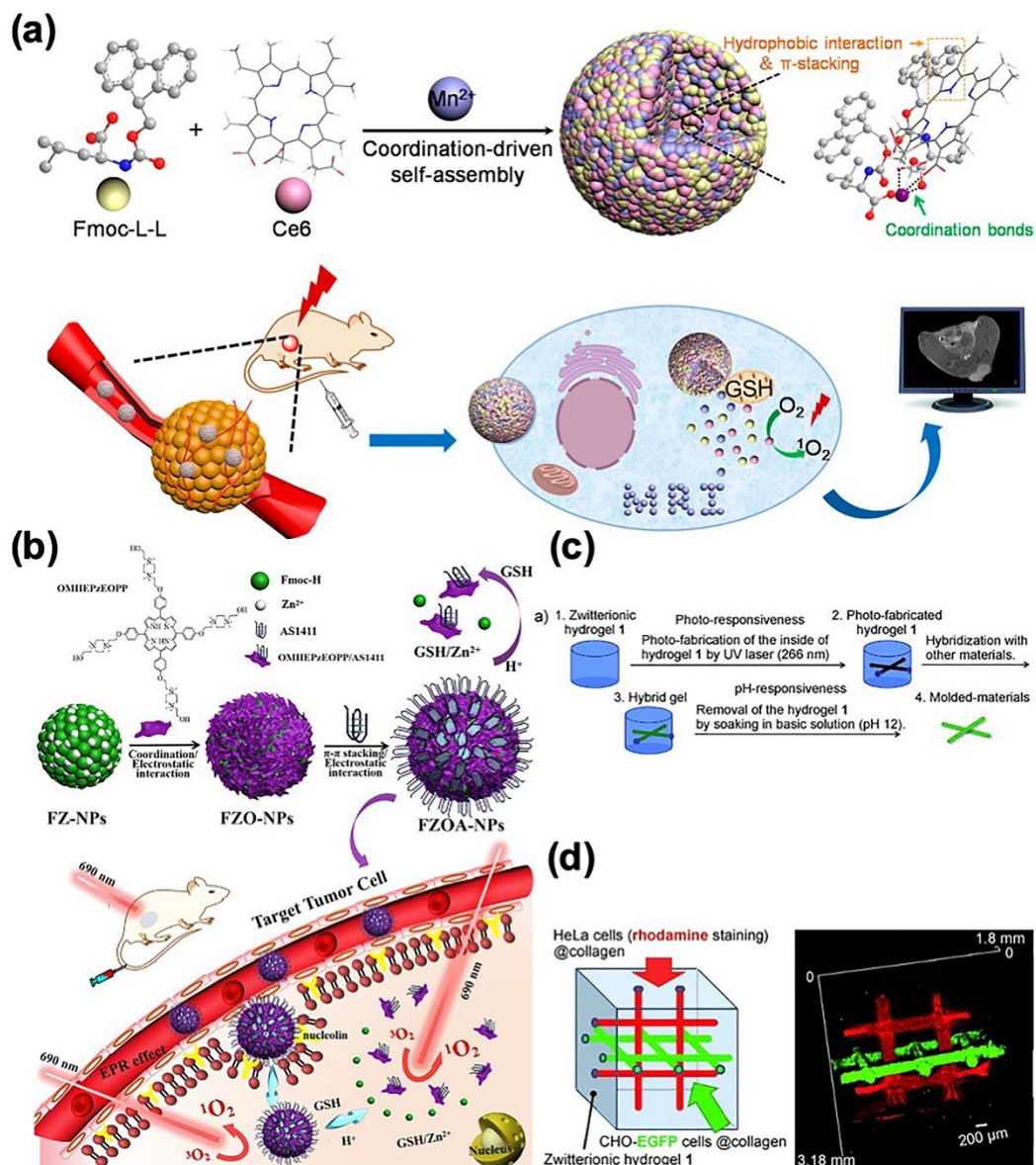


Figure 2. Biomedical applications of nanostructures obtained by the self-assembly of amphiphilic amino acid derivatives. (a) Multifunctional nanoparticles, constituted of Fmoc-leucine and Ce6 with PDT and MRI properties, and exploited for cancer diagnosis and therapy.<sup>47</sup> (b) Nanoparticles composed of Fmoc-histidine and porphyrin photosensitizer, and used for targeted delivery of the porphyrin in the tumor and subsequent PDT.<sup>51</sup> (c) Fabrication of a 2D pattern using a hydrogel as a template.<sup>71</sup> (d) Fabrication of a 3D pattern in a hydrogel for the culture of two types of cells.<sup>71</sup> Reproduced with permission.<sup>47</sup> Copyright 2018, American Chemical Society. Reproduced with permission.<sup>51</sup> Copyright 2020, American Chemical Society. Reproduced with permission.<sup>71</sup> Copyright 2011, Wiley.

Alternatively, reversible changes of supramolecular structures formed by Fmoc-amino acid derivatives can be exploited to design artificial enzymes. In this regard, Huang *et al.* demonstrated the redox-controlled morphology-switching of a Fmoc-phenylalanine selenide derivative.<sup>59</sup> An amphiphilic molecule, synthesized by esterification of Fmoc-phenylalanine with 2,2'-selenodiethanol, could self-assemble into 30-80 nm size nanoparticles with a multi-layer structure in water (Table 1, entry 12). Upon adding cumene hydroperoxide, the free hydroxyl group of the selenide linker was oxidized to selenoxide, leading to a supramolecular architecture change from nanoparticles to nanotubes with ~12.6 nm width and micron scale in length (Fig. 1f). This transformation was reversible and spherical structures were obtained again when reducing selenoxide to selenide by GSH (Fig. 3a). Circular dichroism and fluorescence emission spectroscopy showed that the self-assembly of the selenide and selenoxide derivatives was mainly driven by anti-parallel  $\pi$ -stacking of the fluorenyl rings of Fmoc and formation of intermolecular H-bonds.<sup>59</sup> The more hydrophilic selenoxide had the potential to form additional H-bonds between the Se=O bond and the terminal hydroxyl group resulting in the nanotube formation (Fig. 3b). The nanotubes were composed of a single molecular layer and their external and inner dimensions were 12.5 and 4.5 nm, respectively, while their length was in the micrometer scale. Glutathione peroxidase (GPx) is an enzyme able to scavenge organic hydroperoxides by using GSH as a reducing substrate, allowing to maintain the dynamic balance of ROS into the cells. However, GPx has some limitations related to its high cost, low activity, and poor stability. Therefore, developing artificial GPx mimetics has drawn a certain attention. In this context, the nanoparticles and nanotubes exhibited a structure-dependent activity of GPx. Indeed, the nanotubes showed a higher GPx activity compared to the nanoparticles, probably because the multilayer structure of the nanoparticles covered the selenium inside, while the single layer of the nanotubes made the selenium exposed onto the surface. This study illustrates how further modifications of Fmoc-amino acids can impart novel properties to the self-assembled structures. All these examples indicate that Fmoc-amino acid-mediated co-assembly is a powerful method with possible integration of various functional molecules and high biocompatibility.<sup>45,47,51-53,57-59</sup>

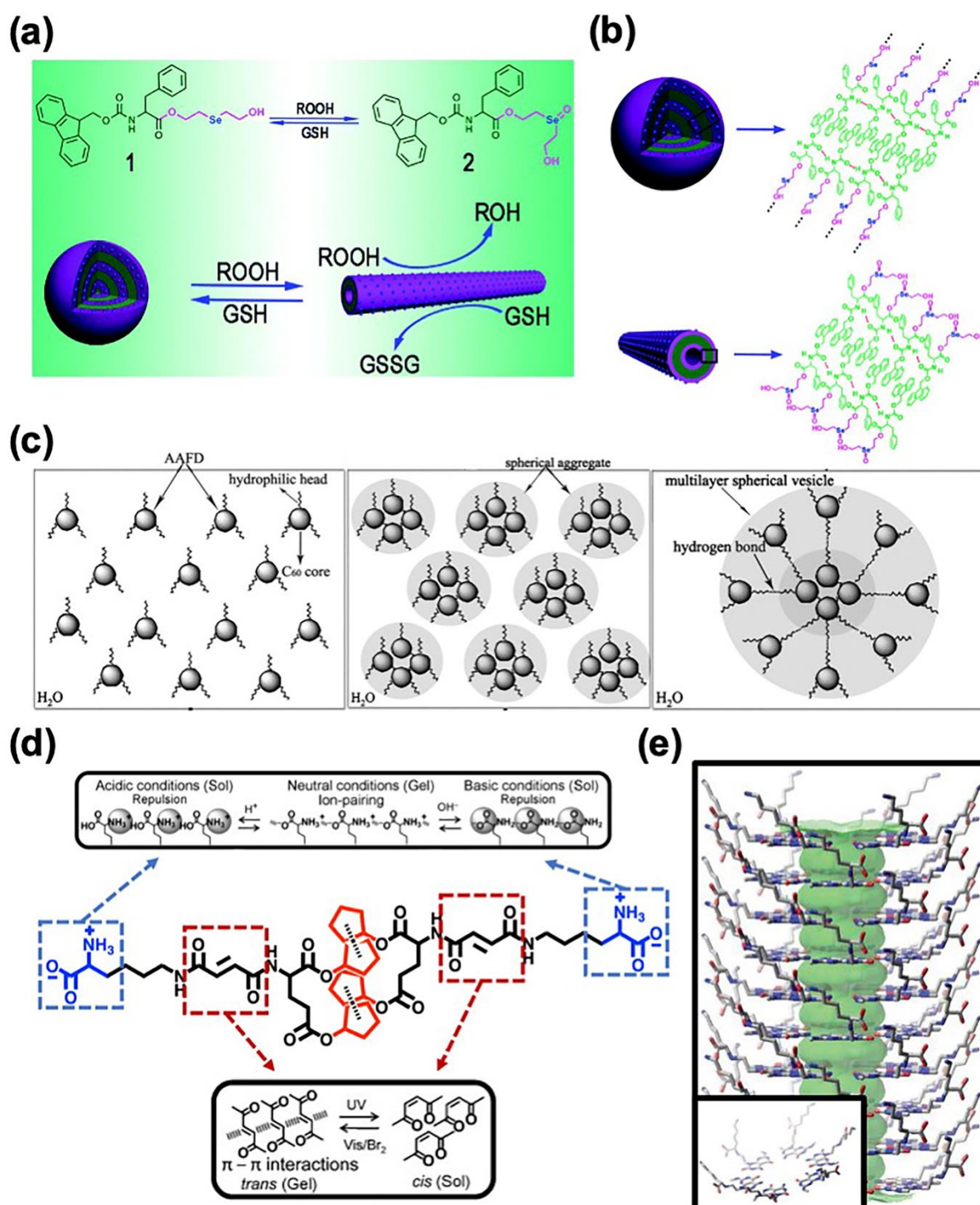


Figure 3. Molecular arrangements and self-assembly mechanisms of amphiphilic amino acid derivatives. (a) Redox-induced transition between nanoparticles and nanotubes formed from Fmoc-phenylalanine esterified with 2,2'-selenodiethanol.<sup>59</sup> (b) Speculative molecular arrangements in the nanoparticles and nanotubes. Additional H-bonds between the Se=O bond and the terminal hydroxyl group contributed to the formation of the nanotubes.<sup>59</sup> (c) The aggregation of C<sub>60</sub> cores (represented as balls) driven by hydrophobic interactions and H-bonds

between the amino and carboxyl groups of the amino acid resulted in the formation of large multilayer vesicles.<sup>67</sup> (d) Structure of gel 1 monomer constituted of a pH-sensitive zwitterionic head, fumaric C=C bonds endowing the molecules with light-induced conformation transition properties, and cyclopentane tails providing hydrophobic interactions.<sup>71</sup> (e) Layer-by-layer stacking of six-membered supermacrocycles forming a rosette nanotube.<sup>73</sup> Reproduced with permission.<sup>59</sup> Copyright 2014, the Royal Society of Chemistry. Reproduced with permission.<sup>67</sup> Copyright 2008, Elsevier. Reproduced with permission.<sup>71</sup> Copyright 2011, Wiley. Reproduced with permission.<sup>73</sup> Copyright 2011, Dove Medical Press (Open access).

### 2.3. Fullerenes

Carbon nanomaterials including carbon nanotubes, graphene, and fullerenes have drawn many attentions during the past decades.<sup>60-62</sup> Specifically, fullerene derivatives can self-assemble into various supramolecular structures with excellent antioxidant properties.<sup>63,64</sup> Due to the electron-accepting ability of the carbon sphere, fullerenes are efficient scavengers of oxidants, such as peroxides. In this context, amphiphilic amino acid-fullerene derivatives, with fullerene as the hydrophobic moiety, were used as antioxidants. As an example, Bjelakovic *et al.* studied the structure and the antioxidant properties of a series of  $\gamma$ -aminobutyric acid (GABA) and glycine-based amphiphilic fullerene derivatives (Table 1, entry 13).<sup>65</sup> Depending on the length and the number of glycine and GABA moieties, as well as the type of solvent, diverse supramolecular micro- and nanostructures were obtained, including nanorods (Fig. 1g), flower-like (Fig. 1h), leaf-like, spiral-like (Fig. 1i), artichoke-like structures (Fig. 1j), flat nanoparticles and curled nanosheets. It was speculated that the molecules first aggregate into spherical particles and then grow to more complexed structures driven by H-bonds and  $\pi$ -stacking. Using the ferrous ion oxidation-xylenol orange assay, the amphiphilic fullerenes showed a higher antioxidant effect than vitamin C and C<sub>60</sub> alone, likely due to an enhanced solubility after amino acid conjugation.<sup>65</sup>

Amphiphilic fullerene derivatives were alternatively prepared by substitution of chlorofullerene (C<sub>60</sub>Cl<sub>6</sub>) with five molecules of 4-aminobutyric acid (R1), glutamic acid (R2), or phenylalanine (R3) methyl ester molecules to generate C<sub>60</sub>R<sub>5</sub>Cl (Table 1, entry 14).<sup>66</sup> They could self-assemble into hollow spherical vesicles with a bilayer shell (3 nm thickness) similar to that of cell membranes (Fig. 1k). The type of amino acid on the fullerene slightly affected the vesicle size (R1 ~140 nm, R2 ~110 nm, and R3 ~90 nm), probably because of the different molecular size of the amino acids. The hydrophobic fullerene moiety was buried inside the

vesicle shell because of hydrophobic and  $\pi$ - $\pi$  interactions, whereas the ester and amino groups were exposed to water thanks to H-bonds and hydrophilic interactions. Anticancer drugs, like 5-fluorouracil, cyclophosphamide, or cisplatin, were loaded inside the vesicles and slowly released. The release rate was dependent on the polarity of the side chains on the fullerene because of the different dipole-dipole force between the side chains and the loaded drugs.<sup>66</sup>

Another type of amino acid fullerene derivative forming vesicles was used to scavenge ROS into the cells. In this case, the fullerene-based amphiphilic molecules were constituted of seven  $\beta$ -alanine, five cystine, or eight arginine moieties (Table 1, entry 15).<sup>67</sup> The amphiphiles could self-assemble in water into spherical structures driven by hydrophobic interactions between the  $C_{60}$  cores. The size of the  $\beta$ -alanine-fullerene nanoparticles was  $\sim 10$  nm, while the cystine- and arginine-fullerene aggregates were bigger ( $\sim 135$  and  $377$  nm, respectively). The diversity in size was attributed to H-bonds in cystine- and arginine-fullerenes, mediating aggregation of small spheres to multilayer vesicles, whereas the  $\beta$ -alanine-fullerene aggregates remained small because of hydrophobic and  $\pi$ - $\pi$  interactions only (Fig. 3c). The fluorescence of the amino acid-fullerene derivatives was enhanced compared to  $C_{60}$  because of the change of the icosahedral symmetry into a distorted conformation due to the covalent modification with the amino acids.<sup>67</sup> Moreover, thanks to their ROS scavenging capacity, these molecules could protect cells from ROS damaging and apoptosis without cytotoxicity. The efficiency of ROS scavenging was dependent on the number of C=C bonds in  $C_{60}$  and the self-assembled structures. The more C=C bonds remained in  $C_{60}$ , the more  $C_{60}$  was exposed to the vesicle surface, thus increasing the ROS scavenging efficiency. The  $\beta$ -alanine-fullerene displayed the best antioxidant effect in cell probably due to its smaller size, allowing easier cellular internalization. Overall, amphiphilic amino acid-fullerenes have great potential in the biomedical field as drug delivery systems and ROS scavengers.<sup>65-67</sup>

Besides fullerenes, carbon nanotubes and graphene-based materials have been also widely explored in the biomedical field due to their unique physicochemical properties, reduced toxicity and biodegradability.<sup>62,68,69</sup> However, these materials have not been combined with single amino acids for self-assembly purposes and biomedical applications. In addition, different from fullerenes, carbon nanotubes and graphene are generally regarded as nanomaterials rather than well-defined molecules. The modification by single amino acids to endow these materials with distinct properties could open the way to the development of new biomedical tools.<sup>70</sup>

## 2.4. Cyclic hydrophobic moieties

Cyclic hydrophobic groups such as cyclic hydrocarbons, aryl and heterocyclic compounds can extend the library of amphiphilic amino acid derivatives with the capacity to self-assemble into various structures, including nanofibers, nanotubes, and nanoparticles. For instance, a series of amino acid derivatives with different hydrophilic head groups and hydrophobic cyclic tails could self-assemble into nanofibers, leading to the formation of hydrogels.<sup>71</sup> In this context, zwitterionic amino acid derivatives were synthesized through connecting lysine and glutamic acid by a fumaric acid linker on the amino side chain (Table 1, entry 16). The two carboxyl groups of the glutamic acid moiety were modified with cyclopentane by esterification (termed gel 1). By replacing the zwitterionic head with saccharide moieties, two glycolipid-type molecules were synthesized, leading to the formation of hydrogels (termed gel 2 and gel 3). Gel 2 contained a fumaric linker and cyclohexane tails, while gel 3 was modified with a succinic acid linker and methylcyclopentane tails. The three hydrogels displayed a different stiffness (gel 1 > gel 2 > gel 3), indicating that ion-pairing and  $\pi$ -stacking are important for mechanical reinforcement. Gel 1 exhibited multiple responsiveness to pH, light, and temperature. The hydrogels formed only at neutral pH and were transformed to fluid solutions in acidic and basic conditions. The reversible pH-sensitivity was due to the zwitterionic head, being in the zwitterionic form at neutral pH and forming a network by electrostatic interactions.<sup>71</sup> However, in acidic or basic conditions, either the amino or the carboxyl ionization, respectively, disrupted the network due to electrostatic repulsion. Additionally, the fumaric C=C bond endowed gel 1 with responsivity to UV light. Indeed, the configuration of the C=C bond switched from *trans* to *cis* upon UV light irradiation, resulting in the breaking of H-bonds followed by gel-sol transition (Fig. 3d). Gel 1 also exhibited thermal responsivity, as the hydrogel turned into a solution at  $\sim 100^\circ\text{C}$  and formed again upon cooling down. Benefiting from stiffness and multiple responsiveness, gel 1 could be used as a template to fabricate various 2D and 3D patterns for cell culture and cell differentiation. Channels in gel 1 were easily constructed through a spatially controlled UV irradiation and etching process. Biocompatible materials like collagen could be injected into the channels, followed by the removal of gel 1 template in basic solution (Fig. 2c). Moreover, the stiffness of gel 1 made the fabrication of 3D patterns possible by constructing multiple interpenetrating channels for different cell types (Fig. 2d). This work showed that gel 1 has a great potential for applications in regenerative medicine.<sup>71</sup>



Different from cyclic alkyl tails, aryl and heterocyclic moieties can provide not only hydrophobic and van der Waals forces, but also strong  $\pi$ - $\pi$  interactions to promote self-assembly. In this context, *N*-benzoyl-L-tyrosine ethyl ester was found to aggregate into uniform nanoparticles in water under a long-time ultrasonication (Table 1, entry 17).<sup>72</sup> The ultrasonic bubbles containing HO• and H• radicals, generated from the thermal decomposition of water vapour and leading to the formation of hydrogen peroxide and superoxide ions, could induce an oxidation of the phenol moiety, resulting in crosslinking to dimers and oligomers forming ~220 nm spherical nanoparticles. In contrast, non-modified tyrosine mostly generated hydroxylated products instead of dimers under the same condition, probably because the crosslinking reaction took place at the gas-liquid interface. The hydrophobic benzoyl moiety helped the tyrosine derivative to aggregate at the interface, while the more hydrophilic non-modified tyrosine was free in solution. Moreover, fluorescence spectroscopy suggested that  $\pi$ - $\pi$  interactions involving the aromatic moieties played an essential role in initiating the self-assembly of the crosslinked oligomers. The nanoparticles displayed fluorescent and antioxidant properties because of  $\pi$ -stacking between oligomers and extensive hydroxylation of the phenyl side chain, respectively, which could be exploited for imaging and therapy.<sup>72</sup>

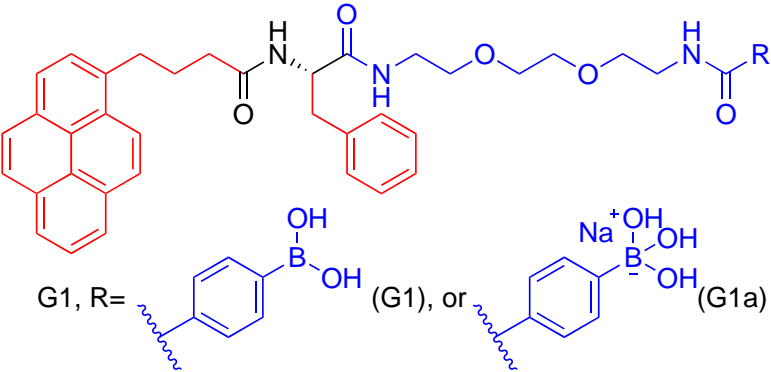
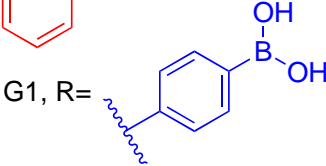
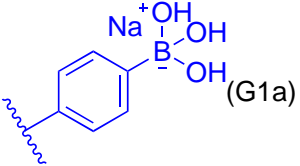
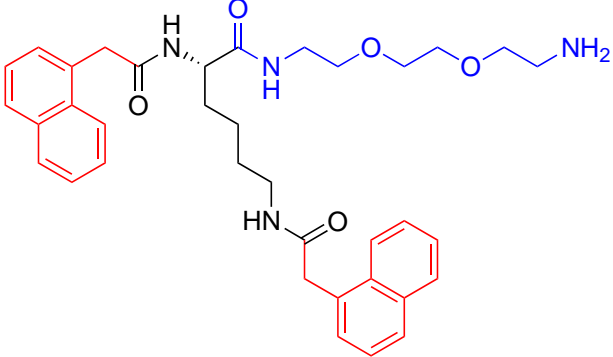
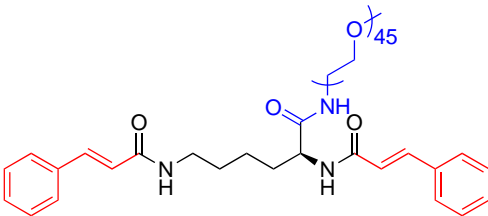
Besides nanofibers and spherical nanoparticles, rosette nanotubes, which are composed of DNA nucleobases guanine and cytosine self-assembled into tubular structures *via* H-bond arrays, were also designed. The  $\alpha$ -amine of lysine was conjugated to a bicyclic moiety possessing the Watson-Crick donor-donor-acceptor H-bond array of guanine and the acceptor-acceptor-donor of cytosine (Table 1, entry 18).<sup>73</sup> In addition to hydrophilic and  $\pi$ - $\pi$  interactions, H-bonds, electrostatic forces, and base-stacking interactions participated to the self-assembly process, leading to the formation of a six-membered supermacrocycle maintained by 18 H-bonds (Fig. 3e). The flat bicyclic moieties in the supermacrocycle could stack layer upon layer to generate rosette nanotubes (Fig. 11).<sup>74</sup> The lysine side chains extending outside the nanotubes imparted stability, biocompatibility, chirality, hydrophilicity, and the possibility of chemical modification. The hydrophobic inner channel was loaded with the hydrophobic drug dexamethasone, an anti-inflammatory and a bone growth promoting steroid molecule. The release of the drug in physiological conditions was very long (up to 9 days). Dexamethasone encapsulated in the rosette nanotubes could induce differentiation of bone marrow-derived stem cells and promote bone growth, thus showing potential for bone tissue engineering.

### **3. Amino acid derivatization with hydrophilic moieties**

Hydrophobic amino acids can be modified by hydrophilic moieties, such as polyethylene glycol (PEG) or chitosan, to design amphiphilic systems. The type of amphiphilic molecules, the self-assembled structures, and their use for biomedical applications are detailed in this section and summarized in Table 2.

Table 2. Amphiphilic amino acid derivatives modified by hydrophilic moieties or by both hydrophobic and oligoethylene glycol chains.

Entry	Amino acids	Molecular structures	Self-assembled structures	Applications	Ref.
The main hydrophilic and hydrophobic moieties are highlighted in blue and red, respectively.					
1	Ala Pro Trp Leu	<p>R = CH<sub>3</sub> or  or </p>	Nanoparticles	Letrozole loading and anticancer activity <i>in vitro</i>	75
2	His Arg <sup>a</sup>		Nanoparticles	pH-sensitive release of doxorubicin and anticancer activity <i>in vitro</i>	78
3	Cys		Bilayer membrane vesicles	pH-sensitive release of methylene blue, calcein, and 1,6-diphenyl-1,3,5-hexatriene	80

4	Phe	 <p>G1, R =  (G1), or  (G1a)</p>	Fibers (hydrogels)	Glucose detection and glucose-sensitive release of insulin	82
5	Lys		Nanofibers (hydrogels)	Antibacterial properties	83
6	Lys		Micelles transformed to hydrogels when adding $\alpha$ - cyclodextrin	Sustained release of DOX	84

7	Ser		Micelles	Doxorubicin and zinc phthalocyanine loading, chemo/PDT cancer therapy <i>in vivo</i>	85
8	Ala Phe Trp		Nanofibers (hydrogels)	Antibacterial properties	86

a: The chemical structure has been corrected from the original figure.

### 3.1. Chitosan

Compared with hydrophilic polymeric chitosan, a single amino acid cannot provide sufficient hydrophobic interactions and the unbalanced ratio between hydrophilic and hydrophobic parts would affect the self-assembly process. Therefore, chitosan-based amphiphilic amino acid derivatives can be designed by grafting amino acids onto the glucosamine moieties. For example, amphiphiles were generated by conjugating chitosan with hydrophobic amino acids, including alanine (A-chitosan), proline (P-chitosan), or tryptophan (W-chitosan), through amidation between the  $\alpha$ -carboxylate of the amino acids and the glucosamine groups (Table 2, entry 1).<sup>75</sup> These molecules could self-assemble into homogeneous nanoparticles with a hydrophobic core and a size depending on the type of amino acid (~250 nm for A-chitosan and W-chitosan, and ~125 nm for P-chitosan). The anticancer drug letrozole was successfully loaded into the nanoparticles thanks to H-bonds and hydrophobic, van der Waals, and  $\pi$ - $\pi$  interactions. Another significant factor for efficient letrozole loading was the steric constraint due to distorted polymer chains wrapping the drug molecules. The drug release kinetics was affected by many parameters, including the drug concentration, the type of amino acid, and the molecular interactions between the drug and the amino acid. An elevated drug concentration resulted in a high diffusion rate and the amino acids interacted differently with the drug. Indeed, depending on the type of amino acid, the self-assembly of the amphiphilic chitosan derivatives led to a different distribution of the hydrophobic domain, either in the core or on the surface of the nanoparticles, which could influence the localization of the drug, either trapped in the core or adsorbed on the surface.<sup>75</sup> For example, compared to A-chitosan and W-chitosan, P-chitosan exhibited a lower release at a lower drug concentration because the hydrophobic interactions between letrozole and the pyrrolidine ring of proline were stronger than the alanine and tryptophan side chains. However, the fastest release at a high drug concentration was occurring because P-chitosan had the lowest capacity of trapping the drug in the core, and more drug adsorbed onto the surface resulted in a faster release. Importantly, the nanoparticles without the drug were biocompatible, whereas the cytotoxic activity of the letrozole-loaded nanoparticles was higher in cancer cells compared to the free drug. Thus, these nanoparticles can be used as safe hydrophobic drug carriers. This work indicates that amphiphilic molecules with a high hydrophobicity can facilitate the loading of hydrophobic drugs and delayed their release.<sup>75</sup>

Similarly, the carboxylic acid of leucine was coupled to the amine of chitosan, the isopropyl side group of leucine providing the hydrophobic character (Table 2, entry 1).<sup>76</sup> Solid

nanoparticles were obtained by water-in-oil emulsification and subsequent crosslinking using glutaraldehyde. Dynamic light scattering evidenced a trimodal size distribution (~1, 30, and 500 nm) with an average hydrodynamic diameter of ~19 nm due to the tendency of the nanoparticles to agglomerate. Diltiazem hydrochloride, an antihypertensive drug, was loaded into the nanoparticles, which were formulated as a dry powder inhaler for pulmonary delivery. The modification of chitosan by leucine made the nanoparticle surface alterable in different conditions. The conformation of the nanoparticles switched from hydrophobic in air (for aerosolization) to hydrophilic in water (for drug delivery) (Fig. 4a). In the dry powder state (in air environment for aerosolization), the surface of the nanoparticles was more hydrophobic than that of the naked chitosan nanoparticles due to the hydrophobic isopropyl group of leucine, which helped to reduce the cohesion of the nanoparticles and to improve their dispersibility.<sup>76</sup> Moreover, the leucine moiety also increased the surface charge, furtherly enhancing the dispersibility. By contrast, in water the leucine residue curled inward, and the hydrophilic amine and amide moieties of leucine were exposed to water, thus increasing the hydrophilicity. When compared to unmodified chitosan nanoparticles, the leucine-based nanoparticles exhibited an improved drug loading efficiency and better release performance (Fig. 4a). The increase of drug loading led to the higher the drug concentration gradient between the nanoparticles and the environment, which increased the diffusional force and amount of drug released. Moreover, the side chain of leucine generated a hydrophobic barrier, trapping the drug and slowing down the release rate, thus enabling sustained release. Overall, the leucine-chitosan nanoparticles endowed of good aerosolization properties, sustained drug release, and high biocompatibility<sup>77</sup> provide opportunities for pulmonary administration of drugs.<sup>76</sup>

Using a similar approach, two different amino acids, *N*-acetyl histidine (NAcHis) and arginine as hydrophobic and hydrophilic moieties, respectively, were coupled to chitosan (Table 2, entry 2).<sup>78</sup> The conjugate self-assembled into nanoparticles and their properties were tuned by changing the substitution degree of chitosan with the amino acids. The increase of NAcHis substitution degree led to the decrease of the critical micellar concentration (CMC) and the nanoparticle size (from ~175 to 90 nm) owing to more hydrophobic interactions, resulting in a more compact stacking of NAcHis in the core. In the case of arginine conjugated to chitosan, the amino acid was exposed on the nanoparticle surface due to its hydrophilic properties, and the positive charge of arginine facilitated the cellular uptake of the nanoparticles. In addition, both NAcHis and arginine endowed the nanoparticles with pH-sensitiveness because the amine and guanidine of arginine and the imidazole moiety of histidine were protonated at acidic pH. Increased electrostatic repulsions led to the decomposition of the

hydrophobic core. A hydrophobic anticancer drug, doxorubicin (DOX), was encapsulated in the nanoparticles. The encapsulation efficiency of DOX was higher with increased NAcHis substitution degree, while the drug release rate was decreased, probably because of a larger hydrophobic reservoir and stronger hydrophobic interactions. Additionally, at low pH, the release of DOX was accelerated because of nanoparticle disruption and higher solubility of the protonated drug. Finally, *in vitro* experiments demonstrated that the nanoparticles were biocompatible, whereas the DOX-loaded nanoparticles displayed an enhanced cellular uptake and a higher cytotoxicity in drug-resistant tumor cell lines compared to free DOX.<sup>78</sup> Owing to the natural origin of chitosan and amino acids, amphiphilic chitosan-based amino acid derivatives were shown to generate safe nanoparticles that can be exploited as drug carriers. Meanwhile, the amphiphilic properties ensure a high drug loading efficiency for both hydrophobic and hydrophilic drugs.<sup>75,76,78</sup>

### 3.2. Polyethylene glycol

PEG is a hydrophilic moiety commonly used to form amphiphilic molecules.<sup>79</sup> Recently, an amphiphilic derivative designed by coupling PEG methyl ether (*m*PEG) to cysteine was reported to self-assemble into vesicles with a bilayer membrane (Table 2, entry 3).<sup>80</sup> The derivative was synthesized by a Michael addition reaction between the thiol group of cysteine and *m*PEG methyl ether methacrylate. Both unilamellar small vesicles (~20-80 nm size) and larger aggregates (~200-500 nm size) existed in solutions, attributed to vesicle fusion. Interestingly, different from the behavior of PEG in other derivatives,<sup>81</sup> *m*PEG conjugated to cysteine stretched into the interior of the bilayer membrane, a behavior similar to hydrophobic alkyl chains, because the zwitterionic head groups of cysteine ( $\alpha$ -ammonium and carboxylate) are more hydrophilic than *m*PEG. The self-assembly of the amphiphilic cysteine-PEG derivative was described as spontaneously entropy-initiated process that was similar to the hydrophobicity mediated self-assembly in most alkyl surfactants. In addition, another reason relies on the polarity difference between the zwitterionic head groups and *m*PEG, which was smaller than traditional amphiphiles with alkyl chains. This hypothesis was confirmed by fluorescence probe studies, where a hydrophobic and weak polar environment was detected inside the vesicle membrane. As a result, the derivative with a long *m*PEG chain (1000 Da) showed a lower CMC than the molecule with a shorter PEG chain (300 Da) due to stronger hydrophobic-like interactions. Owing to the zwitterionic amino acid head groups, the self-assembled vesicles exhibited pH-responsiveness. At acidic or basic pH, the head groups



became cationic or anionic, respectively, leading to repulsion and disintegration of the vesicles. Hydrophilic (methylene blue or calcein) and hydrophobic (1,6-diphenyl-1,3,5-hexatriene) model drugs were loaded inside the vesicles. The hydrophilic dyes were encapsulated into the core, while the hydrophobic dye was inserted into the bilayer membranes. A pH-triggered release was observed due to the pH-induced instability of the vesicles. Overall, the PEG-cysteine amphiphiles exhibited a good drug loading capacity and potential as carriers.<sup>80</sup>

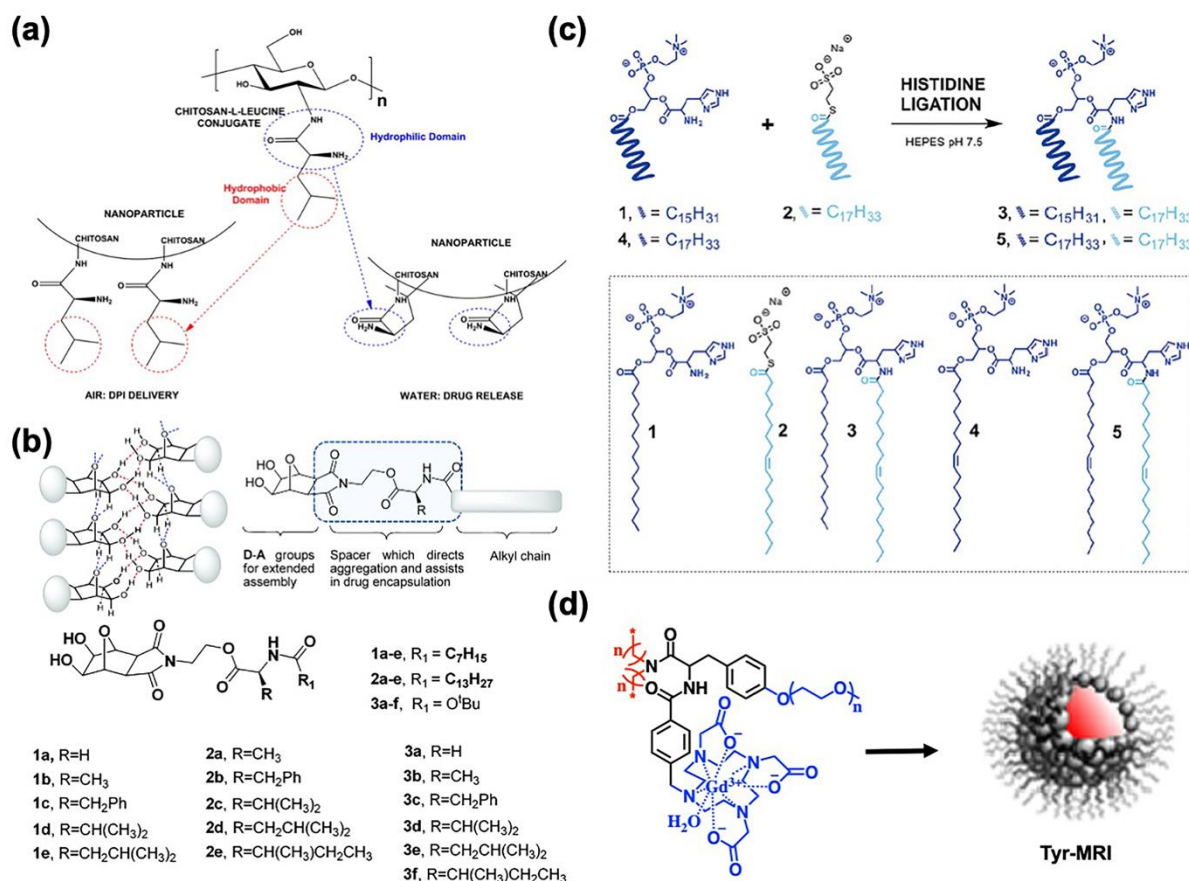


Figure 4. (a) Conformation transition of leucine-grafted chitosan in air and aqueous conditions.<sup>76</sup> (b) Molecular structures and functions of hydroxylated oxanorbornane derivatives. The H-bond network generated by the head groups facilitated the self-assembly process.<sup>87</sup> (c) Molecular structure of compound 1-palmitoyl-2-histidine-sn-glycero-3-phosphocholine (1), 2-mercaptoethanesulfonate oleoyl thioester (2), phospholipid (3), 1-(9-octadecenoyl)-2-histidine-sn-glycero-3-phosphocholin (4), and phospholipid (5).<sup>91</sup> (d) Molecular structure of tyrosine derivatized with Gd-1,4,7,10-tetraazacyclododecane-1,4,7-triacetic acid, able to self-assemble into nanomicelles.<sup>92</sup> Reproduced with permission.<sup>76</sup> Copyright 2016, American Chemical Society. Reproduced with permission.<sup>87</sup> Copyright 2016, the Royal Society of

Chemistry. Reproduced with permission.<sup>91</sup> Copyright 2017, Thieme Medical. Reproduced with permission.<sup>92</sup> Copyright 2018, Wiley.

#### **4. Amino acid derivatization with both hydrophobic and hydrophilic moieties**

The balance between hydrophobic and hydrophilic parts in amphiphilic molecules can affect their self-assembly behavior. In some cases, the intrinsic hydrophilicity or hydrophobicity of amino acids is not very strong in contrast to the grafted moieties. Though out-of-balance amphiphilic molecules could self-assemble into well-defined structures, well-balanced amphiphiles that can be obtained through conjugation of both hydrophobic and hydrophilic groups on the amino acids may present a wider self-assembly capacity. Most derivatives in this section were designed by conjugating long alkyl chains as hydrophobic parts or PEG as hydrophilic parts. The type of amphiphilic molecules, the self-assembled structures, and the biomedical applications described in this section are summarized in Table 2 and Table 3 for the subsections 4.1 and 4.2 focused on oligoethylene glycol chains and long alkyl chains, respectively.

Table 3. Amphiphilic amino acid derivatives with long alkyl and hydrophilic groups or symmetric/bola-structures.

Entry	Amino acids	Molecular structures	Self-assembled structures <sup>a</sup>	Applications	Ref.
1	Gly		R=C <sub>7</sub> H <sub>15</sub> : spheres (methanol), fibers (acetone) R=OtBu: spheres (acetone)		
2	Ala		R=C <sub>7</sub> H <sub>15</sub> : ribbons (methanol), spheres (acetone) R=C <sub>13</sub> H <sub>27</sub> : fibers (methanol) R=OtBu: spheres (acetone)		
3	Phe	-NH-R: R=C <sub>7</sub> H <sub>15</sub> , C <sub>13</sub> H <sub>27</sub> , and OtBu -C(=O)-O-R: R=hydroxylated oxanorbornene	R=C <sub>7</sub> H <sub>15</sub> : spheres (methanol, tetrahydrofuran), vesicles (acetone), ribbons (chloroform and water) R=C <sub>13</sub> H <sub>27</sub> : ribbons (methanol), fibers (acetone) R=OtBu: fibers (acetone)	R1=C <sub>7</sub> H <sub>15</sub> : ibuprofen loading and sustained release	87
4	Val		R=C <sub>7</sub> H <sub>15</sub> : spheres (methanol), vesicles (acetone) R=C <sub>13</sub> H <sub>27</sub> : particles (methanol), fibers (acetone) R=OtBu: spheres (acetone)		
5	Leu		R=C <sub>7</sub> H <sub>15</sub> : spheres (methanol), spheres (acetone) R=C <sub>13</sub> H <sub>27</sub> : flakes (acetone) R=OtBu: spheres (acetone)		
6	Ile				

			R=C <sub>13</sub> H <sub>27</sub> : fibers (methanol), irregular particles (acetone) R=OtBu: spheres (acetone)		
7	Glu	-NH-R: R=pantolactone -C(=O)-O-R: R=octadecylamine	Nanofibers (hydrogels)	Selective adhesion of human serum albumin	90
8	His	-NH-R: R=oleoyl -C(=O)-O-R: R=1-palmitoyl-sn-glycero-3-phosphocholine, 1-(9-octadecenoyl)-sn-glycero-3-phosphocholine	Bilayer membrane microvesicles	Loading of 8-hydroxypyrene-1,3,6-trisulfonic acid and the enhanced green fluorescent protein	91
9	Tyr	-NH-R: R=Gd-1,4,7,10-tetraazacyclododecane-1,4,7-triacetic acid -C(=O)-O-R: R=di-octadecylamine Phenolic OH: PEG <sub>2000</sub>	Core-shell micelles	Magnetic resonance imaging	92
10	His	-NH-R: R=nonanedioic acid	Spherical structures	Glucose sensing	93
11	Lys	-C(=O)-O-R: R=1,12-diaminododecane	Vesicles (co-assembly with Tween-60)	pH-sensitive release of 5-fluorouracil and anticancer activity <i>in vivo</i>	94
12	Phe	-C(=O)-O-R: R=N,N'-disulfanediybis(ethane-2,1-diyl)	Nanoparticles	GSH-sensitive release of indocyanine green and PTT <i>in vitro</i>	95
13	Phe	-NH-R: R=carboxybenzyl -C(=O)-O-R: R=1,4,5,8-naphthalene dianhydride conjugated to a TEG diamine chain	Nanoparticles	Cell imaging, curcumin loading and anticancer activity <i>in vitro</i>	97

14	Tyr	-NH-R: R=tetraphenylethylene Phenolic OH: phosphate	Micelles (pH 7.4) and nanofibers (hydrogels) (pH 2.5)	ALP detection	98
15	Lys, His	-C(=O)-O-R: R=long hydrophobic chain conjugated to histidine, triphenylphosphonium, biotin, or galactose.	Spherical bolosomes (co-assembly with 1,2-dioleoyl-sn-glycero-3- phosphoethanolamine)	DNA transfection, DOX loading	99
16	Phe	-NH-R: R=trimesic core via 6-amino caproic acid (TMA-1), trimesic core (TMA-2) -C(=O)-O-R: R=TEG monomethyl ether (TMA- 1), TEG diamine (TMA-2)	Vesicles	DOX loading	100
17	Lys	-C(=O)-O-R: R=3,5-dimethylbenzene- terminated alkyl chain containing a disulfide bond	Vesicles (co-assembly with pillar[5] arene)	GSH- and pH-sensitive release of mitoxantrone and anticancer activity <i>in vitro</i>	101

<sup>a</sup> In parenthesis is reported the solvent used for the self-assembly

#### 4.1. Oligoethylene glycol chains

A common strategy to impart hydrophilicity to molecules is to graft PEG chains. Different hydrophobic parts, such as aromatic rings, hydrocarbon rings, and polymers can be conjugated to PEG for the synthesis of amphiphilic amino acid derivatives, enabling the formation of micelles and hydrogels. For instance, smart injectable hydrogels with thixotropic self-recovery properties, thermal reversibility, and glucose sensitivity were formed by the self-assembly of a low-molecular-weight amino acid gelator.<sup>82</sup> Thixotropic self-recovery is described as the change of viscosity in a material, in which the viscosity is decreased when the material is disturbed by shaking, sonication, the use of syringes *etc.*, while it is recovered upon resting. In the case of hydrogels, macroscopic thixotropic performance can be obtained by a reversible gel-sol transition through simple shaking. This property is important for injectable hydrogels (Fig. 5a). In this study, the gelator molecule G1 was designed by conjugating phenylalanine to pyrene butyric acid on the amine and to a triethylene glycol (TEG) diamine linker terminated with phenylboronic acid on the carboxyl group (Table 2, entry 4). The sodium salt could form a hydrogel (G1a) in phosphate buffered saline (PBS) solution at physiological pH, whereas hydrogels were obtained using G1 only at basic pH (8.5-12). The G1a hydrogel was constituted of a network of fibers with ~15-20 nm width and micrometer length. H-bonds between the amide and carbonyl groups,  $\pi$ -stacking and hydrophobic interactions between the pyrene moieties played an important role in the hydrogelation. The TEG linker and the phenylboronic acid head group provided the essential hydrophilicity to maintain the suitable HLB for the self-assembly. The molecular arrangement relied on an edge-by-edge or side-to-side *J*-type aggregation. Owing to the intrinsic fluorescence of pyrene and the electron-acceptor properties of the boron atom, G1a could detect glucose in blood, both in the molecular and hydrogel state. In the absence of glucose, the fluorescence of pyrene was quenched by a photoinduced electron transfer from pyrene to boron. Upon addition of glucose, the formation of boronate esters between the boronic acid and the hydroxyl groups of glucose led to the suppression of the photoinduced electron transfer effect, thus resulting in fluorescence recovery (Fig. 5b). Moreover, the binding of glucose could change the HLB of the molecule, increasing the fiber width to ~80-120 nm and inducing hydrogel swelling. The G1a hydrogel was used to load insulin, whose release was found to be triggered by glucose due to a decrease of hydrogel rigidity. Besides, the thixotropic properties of the hydrogel and its good biocompatibility provided opportunities for its use as injectable gel for the treatment of diabetes.<sup>82</sup>

Another type of injectable hydrogel based on an amphiphilic lysine derivative bearing a hydrophilic TEG chain and two hydrophobic aromatic moieties, was also reported.<sup>83</sup> The two amines of lysine were modified with naphthyl groups, while the carboxylic acid was conjugated to TEG diamine (Table 2, entry 5). Hydrogelation of the amphiphilic molecule occurred in dimethyl sulfoxide/phosphate buffer (v/v 1:4). Nanofibers with ~50-130 nm width and micrometer length were formed. The fibrous structures were twisted with each other to generate a 3D network through H-bonds, hydrophobic interactions, and  $\pi$ -stacking. AgNPs were synthesized by *in situ* photoreduction into the hydrogel, where the nanofibers served as both reducing and stabilizing agents. The hydrogel displayed a high mechanical strength and a thixotropic self-recovery, allowing its injection through a syringe, as well as good biocompatibility, attributed to lysine and TEG chain. Owing to the presence of AgNPs, the hydrogel showed antibacterial capacity by exhibiting a high inhibition on both G+ and G- bacteria through the destruction of their membranes. As a result, the hydrogel could find applications as an injectable antibacterial scaffold exploitable in tissue engineering for injury repair.<sup>83</sup>

In another case, based on a similar molecular design, both amino groups of lysine were derivatized with cinnamic acid as a hydrophobic moiety, while long *m*PEG (2000 Da) tails were conjugated onto the carboxylic acid group (Table 2, entry 6).<sup>84</sup> The amphiphilic molecule could self-assemble into ~40 nm core-shell micelles with a hydrophobic core and a hydrophilic shell. The micelles could form a hydrogel upon addition of  $\alpha$ -cyclodextrin. It was hypothesized that  $\alpha$ -cyclodextrin could thread on the *m*PEG tails, forming polypseudorotaxane and generating microcrystalline domains (Fig. 5e). A porous gel structure with a pore size of several micrometers was obtained by the self-assembly of these microcrystals and the aggregation of the hydrophobic domain of the cinnamate moieties. *In vitro* cytotoxicity experiments showed that the hydrogel was safe for cells. DOX was then loaded into the hydrogel, and a slow release was observed, indicating that the hydrogel could be used as a sustained drug delivery platform. Overall, the amphiphiles modified with the short TEG linker in the previous work formed nanofibers, while the modification with long PEG chains increased the HLB of the molecules and formed the micelles.

Besides, an amphiphilic molecule based on a serine core with both hydrophobic and hydrophilic terminals was designed.<sup>85</sup> The amine of serine was conjugated to folic acid, a targeting ligand of cancer cells, while *m*PEG and a hydrophobic poly(propylene sulfide) (PPS) chain were linked to the carboxyl and hydroxyl groups, respectively (Table 2, entry 7). This

amphiphilic molecule could self-assemble into ~ 80 nm micelles with a PPS hydrophobic core. The hydrophobic PPS with a high molecular weight (~7500 Da) facilitated the formation of the micelles and increased their stability. DOX and the photosensitizer zinc phthalocyanine were loaded into the micelles to perform a combined PDT and chemotherapy treatment in tumor-bearing mice, resulting in an efficient tumor accumulation and growth inhibition, and good biocompatibility in normal tissues. PPS showed sensitivity to the ROS generated by the zinc phthalocyanine under laser irradiation at 660 nm. It became hydrophilic because of the oxidation of propylene sulfide into poly-sulfoxides/sulfones by ROS, leading to micelle disassembly and DOX release (Fig. 5c). The ROS have a dual role of inducing apoptosis of cancer cells and triggering micelle disassembly to accelerate the release of DOX.<sup>85</sup>

Cholesterol can be exploited as a hydrophobic part to form amphiphilic molecules. For example, three different amino acids, alanine (1), phenylalanine (2), and tryptophan (3) were linked *via* their carboxyl group to cholesterol through a TEG linker. Their analogous ammonium chloride derivatives were also synthesized (1a, 2a and 3a, respectively), and the hydrogelation capacity of these amphiphiles was evaluated to investigate the relation between the molecular structure and self-assembly properties (Table 2, entry 8).<sup>86</sup> Compound 2 showed an enhanced hydrogelation ability than 1, due to additional  $\pi$ -stacking involving phenylalanine. Additionally, the analogous ammonium chloride derivatives showed better gelation efficiency, probably due to ionic interactions in addition to H-bonds, hydrophobic forces, and also  $\pi$ -stacking in the case of the phenylalanine- and tryptophan-based hydrogels. It is worth noting that 3 could not dissolve in water and failed to form a hydrogel, probably because of a low HLB, whereas 3a could form a hydrogel with the lowest minimum gelation concentration among the different gelators. In this case, the quaternization of the amine allowed reaching an optimum HLB for gelation. Nanofibers with ~40 nm width and micrometer length were observed in hydrogels from 2. Larger mesh-like (~1  $\mu$ m space) and porous networks (~2  $\mu$ m porous) were found in the hydrogels from 2a and 3a, respectively, indicating that stronger interactions led to thicker nanofibers and a denser network in the hydrogel structure.<sup>86</sup> The possible molecular arrangement of the phenylalanine and quaternized tryptophan in the hydrogels was investigated by X-ray powder diffraction. The cholesterol domains stacked with each other, while the hydrophilic ends stretched outwards on each side ordered by H-bonds and  $\pi$ -stacking of the aromatic rings. These aggregates could assemble to a high-ordered packing by layer-on-layer stacking (Fig. 5d). Owing to biologically relevant cholesterol and the amino acids, the hydrogels presented a higher biocompatibility *in vitro* than the hydrogelators



composed of long alkyl chains. Though the ammonium chloride derivatives showed better hydrogelation performance, the absence of free amine group could not provide stabilization for AgNPs. Therefore, AgNPs were *in situ* synthesized in the alanine- and phenylalanine-based hydrogels using sunlight to impart the materials with antibacterial ability against G<sup>+</sup> and G<sup>-</sup> bacteria. This work highlights the importance of using natural molecules, such as amino acids and cholesterol, for generating amphiphilic molecules with high biocompatibility.<sup>86</sup>

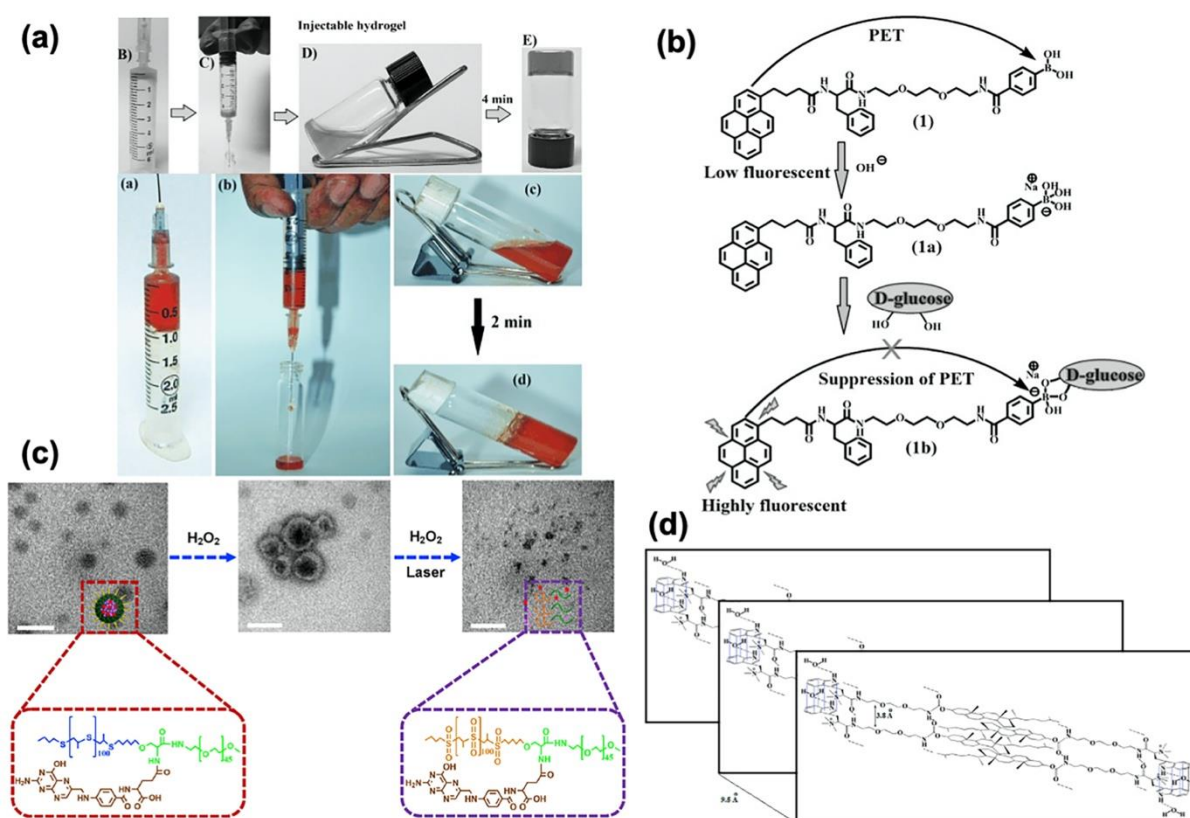


Figure 5. (a) Injectable hydrogels with thixotropic properties: external disturbance like shaking and strain can lead to a gel-sol transition and the solution can be recovered within few minutes.<sup>82,83</sup> (b) Mechanism of glucose detection by suppression of the photoinduced electron transfer (PET) between the pyrene moiety and the phenylboronic acid, and fluorescence enhancement after glucose coupling to the boronic acid moiety.<sup>82</sup> (c) Laser-triggered micelle disassembly and DOX release due to the oxidation of propylene sulfide, increasing the hydrophilicity of the materials.<sup>85</sup> (d) Possible molecular arrangement in hydrogels composed of amphiphilic cholesterol-conjugated amino acids, involving intermolecular stacking and high-ordered packing.<sup>86</sup> Reproduced with permission.<sup>82</sup> Copyright 2015, Wiley. Reproduced

with permission.<sup>83</sup> Copyright 2014, Wiley. Reproduced with permission.<sup>85</sup> Copyright 2016, Elsevier. Reproduced with permission.<sup>86</sup> Copyright 2013, American Chemical Society.

## 4.2. Long alkyl chains

Amino acids cannot only act as spacers in amphiphilic molecules containing long alkyl chains and hydrophilic moieties, but they can also modulate the self-assembly process through their side chain groups. For example, the  $\alpha$ -carboxylate of glycine, alanine, phenylalanine, valine, leucine, or isoleucine was conjugated to a hydrophilic hydroxylated oxanorbornane, while diverse alkyl chains (*e.g.*, *Or*Bu, C-7 or C-13 alkane chains) were coupled to the  $\alpha$ -amine (Fig. 4b and Table 3, entry 1-6).<sup>87</sup> Multiple factors, such as the solvent, the type of alkyl chains, and the amino acid side chains, could influence the self-assembly process. Molecules with C-7 tails formed spherical aggregates (0.3-5  $\mu\text{m}$ ) in acetone, except glycine that formed fibers of several micrometers in length. Only the structures containing alanine could self-assemble into ribbons and fibers with a length of several micrometers in methanol, while other molecules with C-7 tails formed spherical aggregates (0.5-5  $\mu\text{m}$ ) in methanol, even glycine. Similarly, *Or*Bu-terminated molecules aggregated into spherical structures (0.4-5  $\mu\text{m}$ ) in acetone, except phenylalanine (forming fibers). By contrast, molecules with C-13 tails generated more diverse structures, such as flakes, fibers, ribbons, and irregular structures irrespective of the amino acid spacer and the solvent, but no spherical structures. The self-assembly mechanism was not clear, but it was certainly facilitated by the hydrophilic head groups generating a H-bond network and by alkyl chain clustering.<sup>87</sup> Further investigations for phenylalanine and valine spacers with C-7 tails showed that both molecules formed “vesicle-liked” structure in acetone with ~20 nm membrane thickness, which were supposed to be solid nanoparticles with heterogeneous periphery causing by drying or staining. The relationship between the HLB of the molecules and the morphology of the aggregates was studied, indicating that a higher HLB (8.0-10.0) tended to lead to the formation of spherical structures.<sup>87</sup> The molecules with C-7 chains were exploited as carriers of the anti-inflammatory drug ibuprofen. For this purpose, a thin film was formed between the C-7 tailed molecules and ibuprofen, and the film was then hydrated in PBS. In this process, these molecules could self-assemble into vesicles and trap ibuprofen. Cholesterol, known as a stabilizer in niosomes, which are non-ionic surfactant-based vesicles, could increase the stability and rigidity of the vesicles by inserting into the bilayer membrane.<sup>88,89</sup> By introducing cholesterol into the thin film, the drug loading efficiency was higher and the drug release was sustained, without any burst at the initial stage. The amino acid

side chains also influenced the encapsulation efficiency by providing additional  $\pi$ -stacking and hydrophobic interactions with the drug. This study emphasizes the structural variety of different amino acid spacers in amphiphilic molecules.<sup>87</sup>

Multiple alkyl chains can also be used as hydrophobic parts. For instance, the two carboxyl groups of glutamic acid were functionalized with octadecylamine, while the amine was derivatized with chiral pantolactone as hydrophilic part (Table 3, entry 7).<sup>90</sup> The amphiphilic glutamic acid derivative formed hydrogels in an ethanol/water (v/v: 9/1) solution because of the formation of fibrous nanostructures with a width of ~110-150 nm and ~70-100 nm, when glutamic acid was derivatized with D- or L-pantolactone, respectively, and a length of several micrometers. The hydrophobic interaction of alkyl tails and the H-bonds in head groups initiated the self-assembly. Due to the chirality of pantolactone, the two amphiphilic enantiomers displayed distinct properties. For instance, human serum albumin (HSA) exhibited a different adsorption capacity on each enantiotropic hydrogel surface through H-bonds. It was suggested that small differences of interactions at the molecular level could originate when self-assembled into macroscopic materials. Molecular dynamics simulation showed that the D-pantolactone-conjugated glutamic acid fibers were able to penetrate into HSA. On the contrary, the fibers made of the L-amphiphilic derivative could only adhere onto HSA because of cluster formation, resulting in lower adsorption capability of the protein. Therefore, the chirality of the self-assembled amphiphilic chiral glutamic acid derivatives can strongly affect the material properties, in particular the interactions with biological molecules.<sup>90</sup>

In another work, two histidine derivatives were reported to self-assemble into vesicles.<sup>91</sup> The compounds 1-palmitoyl-2-histidine-sn-glycero-3-phosphocholine (1) and 1-(9-octadecenoyl)-2-histidine-sn-glycero-3-phosphocholine (4) were modified by 2-mercaptoethanesulfonate oleoyl thioester (2) on the  $\alpha$ -amine of histidine, generating phospholipids (3) and (5), respectively (Fig. 4c and Table 3, entry 8). The phospholipids contained two hydrophobic long hydrocarbon chains and a hydrophilic zwitterionic phosphocholine head group linked by a glycerol-histidine. They could form microvesicles containing a bilayer membrane. It was proposed that the double alkyl tails on the phospholipids played a significant role in the vesicle formation, because single-tail lysolipids, corresponding to the hydrolyzed lipid derivatives 1 and 2, could only self-assemble into micelles with a size less than 10 nm. Moreover, vesicles were also formed by simply mixing 2 and 4, indicating that the phospholipids could form vesicles, in contrast to the lysolipids. The ability of the vesicles to load biomolecules was verified by encapsulating the fluorescent dye 8-

hydroxypyrene-1,3,6-trisulfonic acid and the enhanced green fluorescent protein. This work provides insights on the formation of vesicles with different sizes using double tail-based amino acid derivatives. Developing simple and effective strategies to mimic the formation of lipid vesicles helps to overcome the challenges related to the generation of artificial membranes.<sup>91</sup>

In another study, tyrosine was exploited as a three-functional scaffold, containing PEG<sub>2000</sub>, two C-18 alkyl chains, and Gd-1,4,7,10-tetraazacyclododecane-1,4,7-triacetic acid, which endowed the tyrosine derivative with amphiphilicity and MRI contrast properties (Fig. 4d and Table 3, entry 9).<sup>92</sup> The amphiphilic molecule could self-assemble in water into spherical core-shell micelles with a diameter of ~11 nm. These micelles exhibited good stability after long time storage at different temperatures (4, 22 and 37°C) and different solvents (water, PBS and saline) but aggregated in cell culture medium. The two C-18 alkyl chains provided hydrophobic interactions for self-assembly. Moreover, similarly to PEG tails, the long alkyl chains also endow the vesicles with blood stability and low hemolysis. Therefore, the micelles displayed a good biocompatibility and prolonged blood circulation, allowing a high contrast of the blood vessels and heart in mice by MRI. Compared with the clinically used small size contrast agent Gd-1,4,7,10-tetraazacyclododecane-1,4,7,10-tetraacetic acid (Gd-DOTA, Dotarem®), these micelles presented high relaxivity and exhibited longer residence time in the vessels, because of their large size and stealth property, thus offering interesting perspectives for MRI of blood vessels.<sup>92</sup>

## **5. Amino acid-based bola-/symmetric amphiphilic structures**

Amphiphilic amino acid derivatives are generally designed by derivatization of their N- and/or C-terminus or their side chain by hydrophilic and hydrophobic domains. Alternatively, amino acid derivatives with a symmetric configuration can form various nanostructures, ranging from nanoparticles to hydrogels. In this context, bola-amphiphilic structures, which contain either hydrophilic or hydrophobic ends and a connecting chain, show special features, such as a high rigidity and stability, when compared with surfactant-like amphiphiles. In addition, other types of molecules can also be designed with centrosymmetric structures containing a core and multiple arms. These new molecular structures have different self-assembly behaviors, leading to the formation of various nanostructures. The type of amphiphilic molecules, the self-assembled structures, and their biomedical applications reported in this section are summarized in Table 3.

## 5.1. Bola-amphiphilic structures

Amphiphilic amino acids can be designed by simply linking two amino acids with an alkyl chain. For instance, two histidine molecules were connected by nonanedioic acid (azelaic acid) through the reaction with the  $\alpha$ -amines to generate a bola-amphiphile (His-C7) (Fig. 6a and Table 3, entry 10).<sup>93</sup> His-C7 could self-assemble into ~200 nm spherical structures in water. The particles were endowed with a peroxidase-like catalytic activity by coordination of the histidine imidazole rings to  $Mn^{2+}$  ions as catalytic sites, without inducing a morphological change. They were utilized as glucose sensors, when combined with glucose oxidase.

In another work, two lysine molecules were linked to 1,12-diaminododecane by amidation (Fig. 6a and Table 3, entry 11).<sup>94</sup> The bola-amphiphilic compound could self-assemble into monolayer vesicles with ~20 nm diameter. Nevertheless, the stability of the vesicles was low, presumably because of the weak interactions between the molecules (absence of  $\pi$ -stacking), which resulted in low drug loading performance. Therefore, in order to strengthen their stability for drug loading and *in vivo* applications, the surfactant Tween-60 was added, and ~20 nm vesicles were formed by H-bonds and hydrophobic interactions. It is worth noting that both Span surfactant and cholesterol failed to form vesicles when co-assembled with the bola-amphiphiles probably due to the unsuitable HLB for Span and the lack of  $\pi$ -stacking, which was critical for the co-assembly. The anticancer drug 5-fluorouracil was loaded into the vesicles and its release could be tuned by pH. Indeed, while the release was delayed under neutral condition, it was accelerated at pH 5.8-6.5. This pH-sensitive drug release could be explained by the protonation of the lysine amines at slightly acidic pH, leading to the vesicle disassembly. The vesicles were not cytotoxic and showed a high potential for tumor treatment in tumor-bearing mice.<sup>94</sup>

Besides simple alkyl chains, functional linkers containing a disulfide bond can be also utilized to connect two amino acids to form bola-amphiphiles. For example, two phenylalanine molecules were linked through the *N,N'*-disulfanediybis(ethane-2,1-diyl) spacer *via* the carboxylic acid moiety of the amino acid (Fig. 6a and Table 3, entry 12).<sup>95</sup> Genipin, a natural crosslinking agent having a high reactivity with primary amine groups, was used to covalently crosslink the amphiphilic bola-amino acids through a reaction with the  $\alpha$ -amines. The genipin-modified bola-amino acids self-assembled in water and formed nanoparticles with an average size of 52 nm. Covalent bonding and strong hydrophobic interactions of the two phenylalanine moieties were considered essential for inducing the self-assembly. The particle size could be regulated by controlling the temperature and pH. The photothermal reagent indocyanine green

(ICG) was loaded in the nanoparticles with a high efficiency and red-shifted absorption to the near-infrared region (808 nm) was observed. The use of carriers for the delivery of ICG allows overcoming the limitations for its use in biomedicine associated to a low stability and a rapid clearance *in vivo*.<sup>95</sup> Owing to the presence of the disulfide bond, the nanoparticles could be degraded by GSH *via* a redox reaction. Benefiting from the higher GSH concentration in cancer cells compared to the extracellular environment,<sup>96</sup> the ICG-loaded nanoparticles were highly stable in serum because of covalent crosslinking, which ensured safe delivery, whereas they were degraded after cellular internalization. A higher photothermal conversion efficiency and an enhanced photostability were found for the nanoparticles loaded with ICG compared to the free molecule. *In vitro* experiments indicated a low cytotoxicity of the nanoparticles and an efficient killing of the tumor cells. Compared with self-assembly driven by noncovalent interactions, the covalent assembly developed in this work demonstrated the formation of stable nanostructures that could be degraded intracellularly to avoid long-term toxicity, which is mandatory for *in vivo* drug delivery.<sup>95</sup> Moreover, this strategy can be applied to other biomolecules containing primary amines to generate versatile nanomaterials by crosslinking using genipin.

The extended aromatic molecules with fluorescence properties, like naphthalene diimide and tetraphenylethylene, can be inserted in spacer to link two amino acid terminals, forming bola-amphiphiles. Besides imparting fluorescence properties to the amphiphiles, additional  $\pi$ - $\pi$  interactions are provided to facilitate the self-assembly. For instance, hydrophobic 1,4,5,8-naphthalene dianhydride was conjugated to TEG diamine terminated with carboxybenzyl-protected phenylalanine (Fig. 6a and Table 3, entry 13).<sup>97</sup> The bola-amphiphilic molecule could self-assemble into spherical nanoparticles with ~30-80 nm size mainly driven by H-bonds (between carbonyl and amide groups) and  $\pi$ -stacking (extended aromatic core and terminal phenyl groups) *via H*-type aggregation, where molecules stack face-to-face. The nanoparticles exhibited a high stability in serum, a low cytotoxicity, and an aggregation-induced emission (AIE) through excimer formation. In free molecular state, weak blue fluorescence was emitted, while it shifted to strong green fluorescence with a long decay lifetime after aggregation into nanoparticles, which provides advantages for cell imaging. Additionally, the absorbance and chiral properties also changed after the self-assembly. The nanoparticles were loaded with the hydrophobic anticancer drug curcumin thanks to  $\pi$ - $\pi$  interactions, and they showed a higher killing efficiency towards cancer cells compared to the free drug.<sup>97</sup>

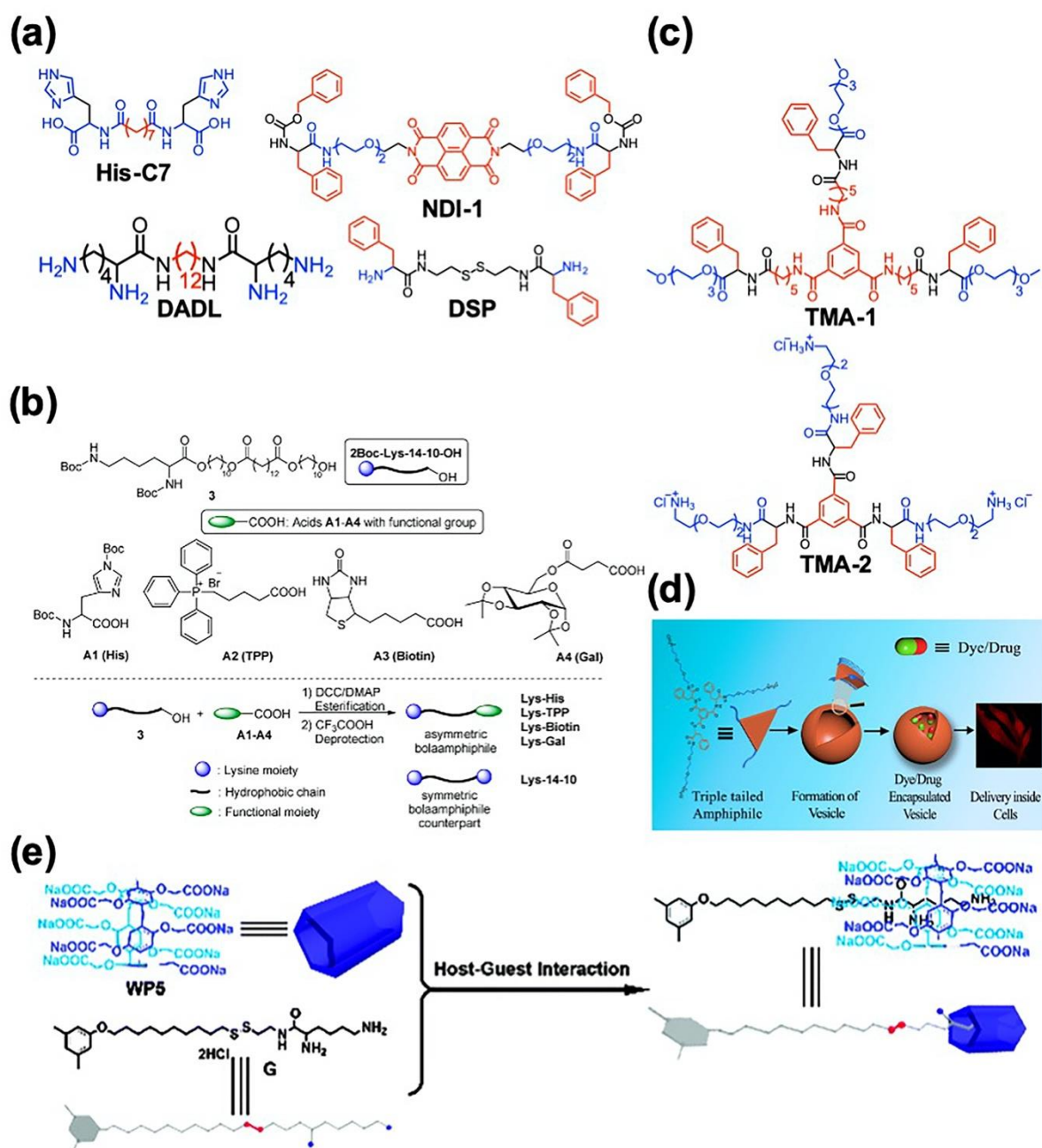


Figure 6. Molecular structures of (a) two histidine molecules connected to azelaic acid (His-C7), two phenylalanine molecules linked through the *N,N'*-disulfanediybis(ethane-2,1-diyl) (DSP), two lysine molecules connected to 1,12-diaminododecane (DADL), and 1,4,5,8-naphthalene dianhydride conjugated to TEG diamine terminated with carboxybenzyl-protected phenylalanine (NDI-1).<sup>93-95,97</sup> (b) Asymmetric bola-type amphiphiles containing lysine and histidine with functional terminals and their brief synthetic route.<sup>99</sup> (c) Structures of the phenylalanine-based triskelion triple-tailed amphiphiles TMA-1 and TMA-2.<sup>100</sup> (d) Vesicles formed from the triple tailed amphiphile by *H*-type aggregation through hydrophobic

interactions and  $\pi$ -stacking.<sup>100</sup> (e) Molecular structure of a water-soluble pillar[5]arene and a hydrophobic lysine derivative, and their host-guest supramolecular complex.<sup>101</sup> Reproduced with permission.<sup>93</sup> Copyright 2015, the Royal Society of Chemistry. Reproduced with permission.<sup>94</sup> Copyright 2017, Elsevier. Reproduced with permission.<sup>95</sup> Copyright 2018, Wiley. Reproduced with permission.<sup>97</sup> Copyright 2017, American Chemical Society. Reproduced with permission.<sup>99</sup> Copyright 2018, Multidisciplinary Digital Publishing Institute (Open access). Reproduced with permission.<sup>100</sup> Copyright 2016, American Chemical Society. Reproduced with permission.<sup>101</sup> Copyright 2015, the Royal Society of Chemistry.

In another example, two tyrosine-phosphate moieties were linked to tetraphenylethylene (Fig. 7a and Table 3, entry 14).<sup>98</sup> The molecule could self-assemble into spherical micelles with ~300 nm size, which were used as probes to detect alkaline phosphatase (ALP), an enzyme overexpressed in cancer cells. The hydrophilic phosphate groups were removed in the presence of ALP and the dephosphorylated molecule exhibited a high hydrophobicity, resulting in aggregation in water and AIE enhanced fluorescence (Fig. 7b). The probe showed a high selectivity for ALP and was used to detect ALP levels in cancer cells. In addition, the tyrosine phosphate-tetraphenylethylene molecule could form nanofibers (~50 nm width and micron scale in length) and hydrogels in acidic conditions driven by  $\pi$ -stacking and hydrophobic interactions between the tetraphenylethylene cores, with an enhanced blue fluorescence due to AIE (Fig. 7c). The micelles were also used as templates to synthesize calcium phosphate microspheres with ~1  $\mu\text{m}$  size by calcium mineralization (Fig. 7d). Overall, the tyrosine phosphate-tetraphenylethylene molecule could potentially be exploited for applications in other fields, including cell imaging, enzyme detection, and drug delivery.<sup>98</sup>

In addition to symmetric bola-type molecular structures, asymmetric bola-type amphiphilic molecules were designed with two different terminal groups, providing additional functions. The C-terminus of lysine was conjugated to different functional molecules, such as histidine, triphenylphosphonium, biotin, or galactose *via* a long hydrophobic chain (Fig. 6b and Table 3, entry 15).<sup>99</sup> Histidine terminal group endowed the molecule with pH-sensitivity. Triphenylphosphonium was used to target mitochondria, while biotin and galactose could facilitate the cellular uptake by ligand-receptor recognition. With the assistance of 1,2-dioleoyl-sn-glycero-3-phosphoethanolamine, spherical bolasomes with ~100 nm size were obtained. Thanks to the protonated amines of lysine, providing DNA binding sites, the bolasomes were



used as DNA transfection agents. Large spherical bolaplexes with ~200-400 nm size were formed after DNA condensation. When compared with the asymmetric bola-amphiphile bearing two terminal lysine, the histidine derivative exhibited the highest cellular transfection efficiency, which was attributed to a better cellular uptake. In addition, histidine has the capacity to promote endosomal escape *via* the proton-sponge effect. Besides, better self-assembly capability was also found for the histidine bola-amphiphile probably due to additional intermolecular forces like  $\pi$ -stacking. In the absence of 1,2-dioleoyl-sn-glycero-3-phosphoethanolamine, the bola-type amphiphiles could self-assemble into spherical aggregates with a size of 20-40 nm. DOX was loaded into the vesicles through hydrophobic interactions for efficient killing of cancer cells *in vitro*. The different self-assembled structures obtained from the bola-type lysine-based amphiphiles find applications as drug delivery systems for gene or drug delivery, and potentially for combined therapies.<sup>99</sup>

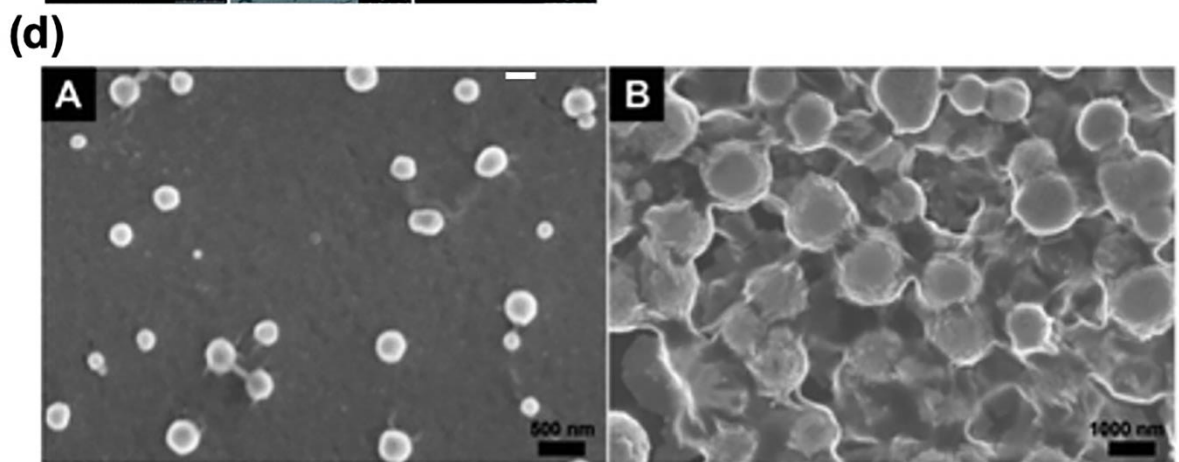
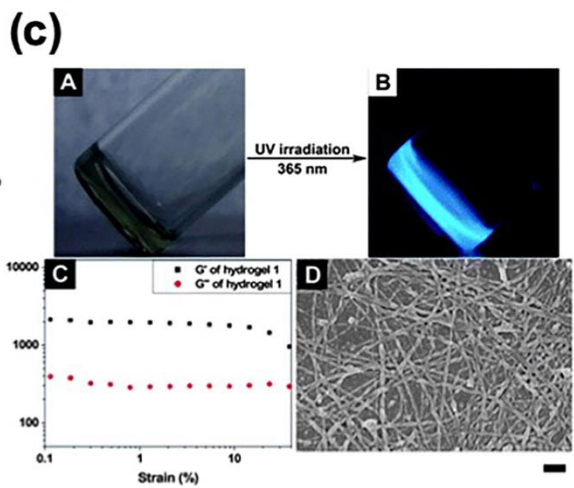
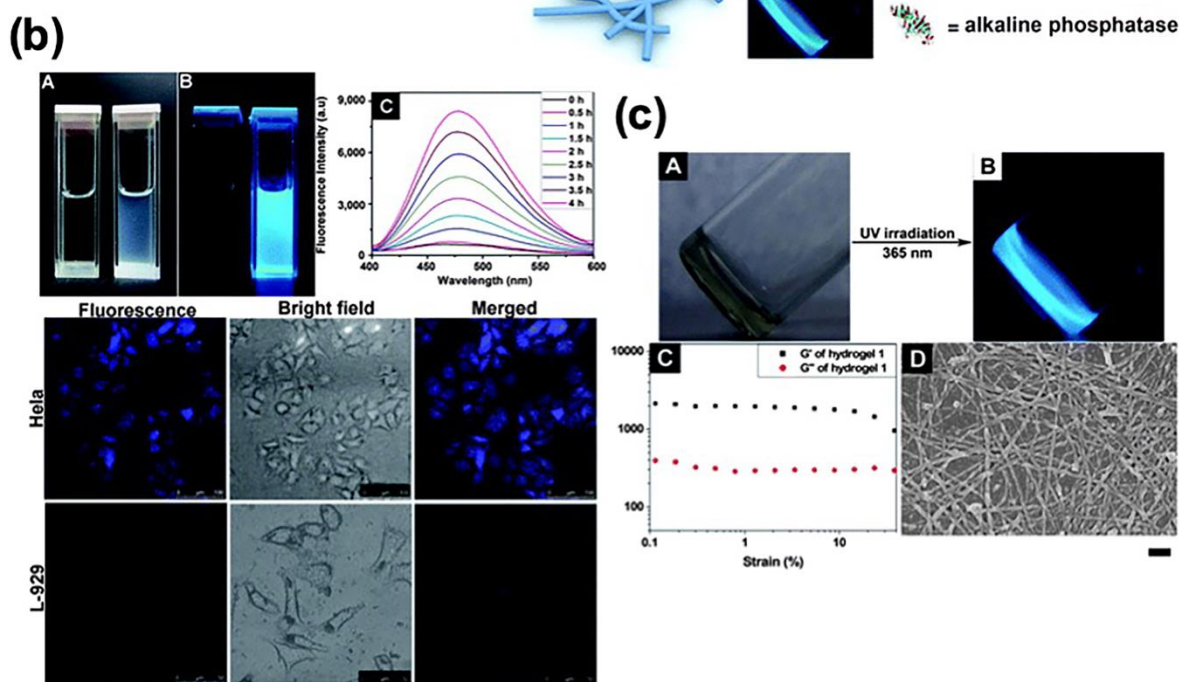
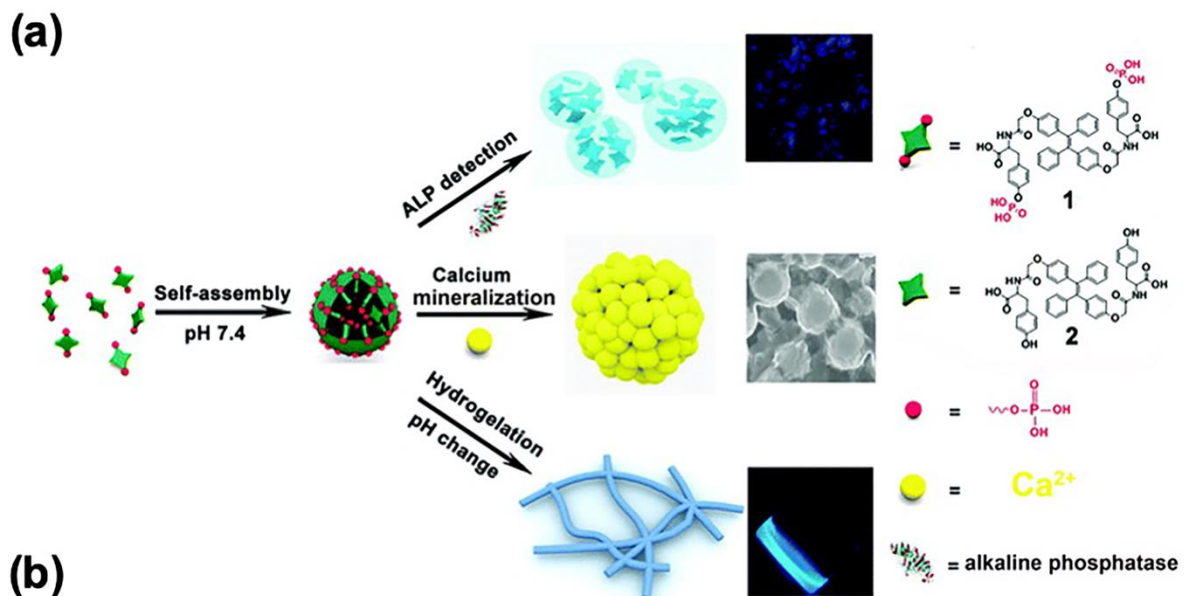


Figure 7. Multifunctional bola-amphiphilic compounds based on tyrosine. (a) Molecular structure of tyrosine phosphate-tetraphenylethylene. Their self-assembled structures can be used for ALP detection, as templates for calcium mineralization, and for the formation of hydrogels. (b) ALP detection by a time-dependent enhanced blue fluorescence. The scale bar is 100  $\mu\text{m}$ . (c) The hydrogels can emit blue fluorescence. TEM images of the hydrogels showing nanofiber structures. The scale bar is 200 nm. (d) Scanning electron microscopy images of tyrosine phosphate-tetraphenylethylene micelles (left) and mineralized microparticles (right).<sup>98</sup> Reproduced with permission.<sup>98</sup> Copyright 2013, the Royal Society of Chemistry.

## 5.2. Centrosymmetric structures

Different from symmetric bola-amphiphiles, centrosymmetric molecules are constituted of a hydrophobic core surrounded by several hydrophilic repeating units. For example, two phenylalanine-based triskelion triple-tailed amphiphiles (TMA) with a hydrophobic trimesic acid (benzene-1,3,5-tricarboxylic acid) core were synthesized (Fig. 6c and Table 3, entry 16).<sup>100</sup> In TMA-1 molecule with neutral side chains, TEG monomethyl ether was conjugated to the carboxylate of phenylalanine, while the  $\alpha$ -amine was linked to the trimesic core *via* 6-amino caproic acid. In contrast, in TMA-2 containing ammonium groups, phenylalanine was directly connected to the core through the  $\alpha$ -amine, whereas the carboxyl function was coupled to TEG diamine. The type of terminal groups affected the self-assembly of the TMA. Indeed, TMA-1 could self-assemble into monolayered vesicles with  $\sim$ 250-300 nm size in a mixture of dimethyl sulfoxide/water (v/v 2:1), while TMA-2 could form  $\sim$ 100-150 nm monolayered vesicles in pure water owing to the presence of the protonated amines. Different from traditional surfactant-like amphiphiles, the molecular arrangement in the monolayer vesicles was due to *H*-type aggregation through hydrophobic interactions and  $\pi$ -stacking (Fig. 6d). The hydrophobic central core exhibited interlamellar orientation and stacked face-to-face. The hydrophilic arms stretched outwards to the aqueous medium to maintain structure stability in solution. The hydrophilic dye calcein was loaded in the vesicles, confirming that the vesicles have an aqueous core. This study was extended to the encapsulation of DOX in TMA-2, suggesting a potential application of the vesicles as drug delivery systems.<sup>100</sup>

In another study, an amphiphilic host-guest compound was designed by the inclusion of a hydrophobic lysine derivative containing a disulfide bond and a 3,5-dimethylbenzene-terminated alkyl chain, in a water-soluble pillar[5]arene bearing five carboxylates (Fig. 6e and

Table 3, entry 17).<sup>101</sup> The inclusion complex could self-assemble in water into vesicles with ~112 nm size driven by the hydrophobic and electrostatic interactions. The vesicles were GSH- and pH-responsive owing to the disulfide bond and the carboxylates, respectively. At pH 5 the carboxylate moieties were protonated, leading to vesicle disassembly and precipitation of the pillar[5]arene. Based on these properties, the vesicles were used as carriers of the anticancer drug mitoxantrone. High loading of mitoxantrone was obtained and the drug-loaded vesicles were larger (~210 nm) than the empty ones. The release of the drug was controlled by pH and the concentration of GSH. Indeed, at low GSH concentration and in neutral conditions, almost no mitoxantrone could leak from the vesicles, whereas an increased GSH concentration and a lower pH allowed accelerating the liberation of the drug. The controlled release of mitoxantrone was promising for treating tumor cells, which have a slightly acidic pH and a relatively high GSH concentration, as an efficient inhibition of the proliferation of cancer cells was observed.<sup>101</sup>

## 6. Conclusions

The self-assembly of amphiphilic amino acid derivatives allows generating a variety of nanostructures, which can be exploited for various biomedical applications, including antibacterial, antitumor, as well as tissue engineering and drug delivery. By introducing hydrophilic, hydrophobic, or aromatic moieties, the self-assembly of amino acids can be promoted through multiple noncovalent interactions. The structure and properties of the amino acids can be easily modulated, as both the carboxylic acid and amino groups can be functionalized in mild conditions. The molecular design not only influences the self-assembled structure by providing different interactions, but also helps to achieve an optimum balance between hydrophilicity and hydrophobicity. Tuning the HLB allows modulating the self-assembly capacity of amphiphilic amino acids, leading to the formation of various nanostructures with distinct properties. Moreover, the molecular structure can also affect the functions and properties of the materials. Beside the direct introduction of functional moieties like sensitive bonds, fluorescent probes and targeting ligands, some functional groups can also influence the material properties by improving biocompatibility and antitumor effect, facilitating drug loading, and imparting AIE fluorescence for instance. The excellent biocompatibility and biodegradability of amino acids give to the nanostructures advantages for bio-related applications, compared to inorganic nanoparticles. Besides, using amino acids with side-chain functions that can be chemically modified, such as lysine, glutamic acid, aspartic acid, cysteine, serine, and tyrosine, makes more sophisticated design possible. However, there

is still large room for the design and applications of amphiphilic amino acid derivatives, not only in biomedicine, but also in other fields such as photocatalysis.<sup>102</sup>

## Acknowledgments

The authors gratefully acknowledge the Agence Nationale de la Recherche (ANR) through the LabEx project Chemistry of Complex Systems (ANR-10-LABX-0026\_CSC). We also wish to thank the Centre National de la Recherche Scientifique (CNRS) and the International Center for Frontier Research in Chemistry (icFRC). TW is indebted to the Chinese Scholarship Council for supporting his PhD internship.

## References

1. J. M. Lehn, *Acc. Chem. Res.*, 1978, **11**, 49-57.
2. J. M. Lehn, *Chem. Scr.*, 1988, **28**, 237-262.
3. European Commission, [https://ec.europa.eu/environment/chemicals/nanotech/reach-clp/index\\_en.htm#:~:text=On%20the%20basis%20of%20the,in%20the%20number%20size%20distribution%2C](https://ec.europa.eu/environment/chemicals/nanotech/reach-clp/index_en.htm#:~:text=On%20the%20basis%20of%20the,in%20the%20number%20size%20distribution%2C), (Accessed September 2020).
4. M. Mauro, A. Aliprandi, D. Septiadi, N. S. Kehr and L. De Cola, *Chem. Soc. Rev.*, 2014, **43**, 4144-4166.
5. S. Sun, *Adv. Mater.*, 2006, **18**, 393-403.
6. Y. Li, Y. Wang, G. Huang and J. Gao, *Chem. Rev.*, 2018, **118**, 5359-5391.
7. David Richards and Albena Ivanisevic, *Chem. Soc. Rev.*, 2012, **41**, 2052-2060.
8. S. J. Soenen, W. J. Parak, J. Rejman and B. Manshian, *Chem. Rev.*, 2015, **115**, 2109-2135.
9. P. Makam and E. Gazit, *Chem. Soc. Rev.*, 2018, **47**, 3406-3420.
10. J. Zhou, X. Du, C. Berciu, H. He, J. Shi, D. Nicastro and B. Xu, *Chem*, 2016, **1**, 246-263.
11. H. S. Azevedo and I. Pashkuleva, *Adv. Drug Delivery Rev.*, 2015, **94**, 63-76.
12. T. Schnitzler and A. Herrmann, *Acc. Chem. Res.*, 2012, **45**, 1419-1430.
13. P. Banerjee, A. Pyne and N. Sarkar, *J. Phys. Chem. B*, 2020, **124**, 2065-2080.
14. B. J. Kim, D. Yang and B. Xu, *Trends Chem.*, 2020, **2**, 71-83.
15. C. Ménard-Moyon, V. Venkatesh, K. V. Krishna, F. Bonachera, S. Verma and A. Bianco, *Chem. Eur. J.*, 2015, **21**, 11681-11686.
16. C. Cai, J. Lin, Y. Lu, Q. Zhang and L. Wang, *Chem. Soc. Rev.*, 2016, **45**, 5985-6012.
17. S. I. Stupp, *Nano Lett.*, 2010, **10**, 4783-4786.
18. H. Hosseinkhani, P. Hong and D. Yu, *Chem. Rev.*, 2013, **113**, 4837-4861.
19. H. Wang, Z. Feng and B. Xu, *Angew. Chem. Int. Ed.*, 2019, **58**, 10423-10432.
20. T. D. Do, W. M. Kincannon and M. T. Bowers, *J. Am. Chem. Soc.*, 2015, **137**, 10080-10083.
21. S. Bera, B. Xue, P. Rehak, G. Jacoby, W. Ji, L. J. W. Shimon, R. Beck, P. Král, Y. Cao and E. Gazit, *ACS Nano*, 2020, **14**, 1694-1706.
22. M. Szeferczyk, E. Węglarz-Tomczak, P. Fortuna, A. Krzysztóń, E. Rudzińska-Szostak and Ł. Berlicki, *Angew. Chem. Int. Ed.*, 2017, **56**, 2087-2091.
23. K. Fosgerau and T. Hoffmann, *Drug Discov. Today*, 2015, **20**, 122-128.
24. P. T. Liu, S. Stenger, H. Li, L. Wenzel, B. H. Tan, S. R. Krutzik, M. T. Ochoa, J. Schaubert, K. Wu, C. Meinken, D. L. Kamen, M. Wagner, R. Bals, A. Steinmeyer, U. Zügel, R. L. Gallo, D. Eisenberg, M. Hewison, B. W. Hollis, J. S. Adams, B. R. Bloom and R. L. Modlin, *Science*, 2006, **311**, 1770-1773.

25. Q. Zou and X. Yan, *Chem. Eur. J.*, 2018, **24**, 755-761.
26. S. Bera, S. Mondal, S. Rencus-Lazar and E. Gazit, *Acc. Chem. Res.*, 2018, **51**, 2187-2197.
27. P. Chakraborty and E. Gazit, *ChemNanoMat*, 2018, **4**, 730-740.
28. M. P. Hendricks, K. Sato, L. C. Palmer and S. I. Stupp, *Acc. Chem. Res.*, 2017, **50**, 2440-2448.
29. K. Tao, A. Levin, L. Adler-Abramovich and E. Gazit, *Chem. Soc. Rev.*, 2016, **45**, 3935-3953.
30. S. Fleming and R. V. Ulijn, *Chem. Soc. Rev.*, 2014, **43**, 8150-8177.
31. L. R. MacGillivray, *Angew. Chem. Int. Ed.*, 2012, **51**, 1110-1112.
32. K. R. Raghupathi, J. Guo, O. Munkhbat, P. Rangadurai and S. Thayumanavan, *Acc. Chem. Res.*, 2014, **47**, 2200-2211.
33. M. Amit, S. Yuran, E. Gazit, M. Reches and N. Ashkenasy, *Adv. Mater.*, 2018, **30**, 1707083.
34. N. Habibi, N. Kamaly, A. Memic and H. Shafiee, *Nano Today*, 2016, **11**, 41-60.
35. D. M. Raymond and B. L. Nilsson, *Chem. Soc. Rev.*, 2018, **47**, 3659-3720.
36. H. Ren, L. Wu, L. Tan, Y. Bao, Y. Ma, Y. Jin and Q. Zou, *Beilstein J. Nanotechnol.*, 2021, **12**, 1140-1150.
37. A. Shome, S. Dutta, S. Maiti and P. K. Das, *Soft Matter*, 2011, **7**, 3011-3022.
38. E. B. Olutaş and M. Acımiş, *J. Chem. Eng. Data*, 2014, **59**, 869-879.
39. A. Roy, M. Maiti, R. R. Nayak and S. Roy, *J. Mater. Chem. B*, 2013, **1**, 5588-5601.
40. D. R. Nogueira, L. E. Scheeren, L. B. Macedo, A. I. P. Marcolino, M. P. Vinardell, M. Mitjans, M. R. Infante, A. A. Farooqi and C. M. B. Rolim, *Amino Acids*, 2016, **48**, 157-168.
41. D. R. Nogueira, M. Mitjans, M. R. Infante and M. P. Vinardell, *Acta Biomater.*, 2011, **7**, 2846-2856.
42. I. S. Oliveira, R. L. Machado, M. J. Araújo, A. C. Gomes and E. F. Marques, *Chem. Eur. J.*, 2021, **27**, 692-704.
43. Y. Wang, L. Jiang, Q. Shen, J. Shen, Y. Han and H. Zhang, *RSC Adv.*, 2017, **7**, 41561-41572.
44. L. Chen, K. Chen, X. Huang, J. Lou, J. Li and S. Deng, *Colloids Surf. B*, 2019, **173**, 69-76.
45. K. Liu, R. Xing, Q. Zou, G. Ma, H. Möhwald and X. Yan, *Angew. Chem. Int. Ed.*, 2016, **55**, 3036-3039.
46. J. Dolai, K. Mandal and N. R. Jana, *ACS Appl. Nano Mater.*, 2021, **4**, 6471-6496.
47. H. Zhang, K. Liu, S. Li, X. Xin, S. Yuan, G. Ma and X. Yan, *ACS Nano*, 2018, **12**, 8266-8276.
48. F. Q. Schafer and G. R. Buettner, *Free Radical Biol. Med.*, 2001, **30**, 1191-1212.
49. J. P. Celli, B. Q. Spring, I. Rizvi, C. L. Evans, K. S. Samkoe, S. Verma, B. W. Pogue and T. Hasan, *Chem. Rev.*, 2010, **110**, 2795-2838.
50. M. Valko, D. Leibfritz, J. Moncol, M. T. D. Cronin, M. Mazur and J. Telser, *Int. J. Biochem. Cell Biol.*, 2007, **39**, 44-84.
51. J. Chu, D. Wang, L. Zhang, M. Cheng, R. Gao, C. Gu, P. Lang, P. Liu, L. Zhu and D. Kong, *ACS Appl. Mater. Interfaces*, 2020, **12**, 7575-7585.
52. J. Han, K. Liu, R. Chang, L. Zhao and X. Yan, *Angew. Chem. Int. Ed.*, 2019, **58**, 2000-2004.
53. R. Geng, R. Chang, Q. Zou, G. Shen, T. Jiao and X. Yan, *Small*, 2021, **17**, 2008114.
54. C. Guilbaud-Chéreau, B. Dinesh, R. Schurhammer, D. Collin, A. Bianco and C. Ménard-Moyon, *ACS Appl. Mater. Interfaces*, 2019, **11**, 13147-13157.
55. A. Y. Gahane, V. Singh, A. Kumar and A. K. Thakur, *Biomater. Sci.*, 2020, **8**, 1996-2006.

56. I. Irwansyah, Y. Li, W. Shi, D. Qi, W. R. Leow, M. B. Y. Tang, S. Li and X. Chen, *Adv. Mater.*, 2015, **27**, 648-654.
57. C. Yuan, A. Levin, W. Chen, R. Xing, Q. Zou, T. W. Herling, P. K. Challa, T. P. J. Knowles and X. Yan, *Angew. Chem. Int. Ed.*, 2019, **58**, 18116-18123.
58. J. Song, C. Yuan, T. Jiao, R. Xing, M. Yang, D. J. Adams and X. Yan, *Small*, 2020, **16**, 1907309.
59. Z. Huang, Q. Luo, S. Guan, J. Gao, Y. Wang, B. Zhang, L. Wang, J. Xu, Z. Dong and J. Liu, *Soft Matter*, 2014, **10**, 9695-9701.
60. K. P. Loh, D. Ho, G. N. C. Chiu, D. T. Leong, G. Pastorin and E. K. H. Chow, *Adv. Mater.*, 2018, **30**, 1802368.
61. X. Cui, S. Xu, X. Wang and C. Chen, *Carbon*, 2018, **138**, 436-450.
62. R. Soltani, S. Guo, A. Bianco and C. Ménard-Moyon, *Adv. Ther.*, 2020, **3**, DOI: 10.1002/adtp.202000051.
63. H. Ma, J. Zhao, H. Meng, D. Hu, Y. Zhou, X. Zhang, C. Wang, J. Li, J. Yuan and Y. Wei, *ACS Appl. Mater. Interfaces*, 2020, **12**, 16104-16113.
64. M. S. Bjelaković, T. J. Kop, M. Vlajić, J. Đorđević and D.R. Milić, *Tetrahedron*, 2014, **70**, 8564-8570.
65. M. S. Bjelaković, T. J. Kop, J. Đorđević and D. R. Milić, *Beilstein J. Nanotechnol.*, 2015, **6**, 1065-1071.
66. M. Lin, R. Chen, N. Yu, L. Sun, Y. Liu, C. Cui, S. Xie, R. Huang and L. Zheng, *Colloids Surf. B*, 2017, **159**, 613-619.
67. Z. Hu, W. Guan, W. Wang, L. Huang, X. Tang, H. Xu, Z. Zhu, X. Xie and H. Xing, *Carbon*, 2008, **46**, 99-109.
68. B. Ma, C. Martín, R. Kurapati and A. Bianco, *Chem. Soc. Rev.*, 2020, **49**, 6224-6247.
69. G. Reina, J. M. González-Domínguez, A. Criado, E. Vázquez, A. Bianco and M. Prato, *Chem. Soc. Rev.*, 2017, **46**, 4400-4416.
70. J. B. Awuah and T. R. Walsh, *Small*, 2020, **16**, 1903403.
71. H. Komatsu, S. Tsukiji, M. Ikeda and I. Hamachi, *Chem. Asian J.*, 2011, **6**, 2368-2375.
72. F. Cavalieri, E. Colombo, E. Nicolai, N. Rosato and M. Ashokkumar, *Mater. Horiz.*, 2016, **3**, 563-567.
73. Y. Chen, S. Song, Z. Yan, H. Fenniri and T. J. Webster, *Int. J. Nanomed.*, 2011, **6**, 1035-1044.
74. H. Fenniri, P. Mathivanan, K. L. Vidale, D. M. Sherman, K. Hallenga, K. V. Wood and J. G. Stowell, *J. Am. Chem. Soc.*, 2001, **123**, 3854-3855.
75. M. Motiei, S. Kashanian and A. A. Taherpour, *Drug Dev. Ind. Pharm.*, 2017, **43**, 1-11.
76. M. D. A. Muhsin, G. George, K. Beagley, V. Ferro, H. Wang and N. Islam, *Mol. Pharmaceutics*, 2016, **13**, 1455-1466.
77. M. D. A. Muhsin, G. George, K. Beagley, V. Ferro, C. Armitage and N. Islam, *Biomacromolecules*, 2014, **15**, 3596-3607.
78. M. A. Raja, M. Arif, C. Feng, S. Zeenat and C. Liu, *J. Biomater. Appl.*, 2017, **31**, 1182-1195.
79. Z. Cao and S. Jiang, *Nano Today*, 2012, **7**, 404-413.
80. R. Ghosh and J. Dey, *Langmuir*, 2014, **30**, 13516-13524.
81. A. Kulkarni, K. DeFrees, S. Hyun and D. H. Thompson, *J. Am. Chem. Soc.*, 2012, **134**, 7596-7599.
82. D. Mandal, S. K. Mandal, M. Ghosh and P. K. Das, *Chem. Eur. J.*, 2015, **21**, 12042-12052.
83. S. K. Mandal, S. Brahmachari and P. K. Das, *ChemPlusChem*, 2014, **79**, 1733-1746.
84. Y. Long, H. Song, B. He, Y. Lai, R. Liu, C. Long and Z. Gu, *J. Biomater. Appl.*, 2012, **27**, 333-344.

85. L. Dai, Y. Yu, Z. Luo, M. Li, W. Chen, X. Shen, F. Chen, Q. Sun, Q. Zhang, H. Gu and K. Cai, *Biomaterials*, 2016, **104**, 1-17.
86. S. Dutta, T. Kar, D. Mandal and P. K. Das, *Langmuir*, 2013, **29**, 316-327.
87. D. S. Janni, U. C. Reddy, S. Saroj and K. M. Muraleedharan, *J. Mater. Chem. B*, 2016, **4**, 8025-8032.
88. I. F. Uchegbu and A. T. Florence, *Adv. Colloid Interface Sci.*, 1995, **58**, 1–55.
89. B. Nasser, *Int. J. Pharm.*, 2005, **300**, 95–101.
90. K. Lv, L. Zhang, W. Lu and M. Liu, *ACS Appl. Mater. Interfaces*, 2014, **6**, 18878-18884.
91. R. J. Brea, A. Bhattacharya and N. K. Devaraj, *Synlett*, 2017, **28**, 108-112.
92. A. Babič, V. Vorobiev, C. Xayaphoummine, G. Lapiorey, A. Chauvin, L. Helm and E. Allémann, *Chem. Eur. J.*, 2018, **24**, 1348-1357.
93. M. Kim and S. Lee, *Nanoscale*, 2015, **7**, 17063-17070.
94. B. Hu, Y. Yuan, Y. Yan, X. Zhou, Y. Li, Q. Kan and S. Li, *Mater. Sci. Eng. C*, 2017, **75**, 637-645.
95. Y. Liu, L. Zhao, R. Xing, T. Jiao, W. Song and X. Yan, *Chem. Asian J.*, 2018, **13**, 3526-3532.
96. J. A. Cook, H. I. Pass, S. N. Iype, N. Friedman, W. DeGraff, A. Russo and J. B. Mitchell, *Cancer Res.*, 1991, **51**, 4287-4294.
97. P. Choudhury, K. Das and P. K. Das, *Langmuir*, 2017, **33**, 4500-4510.
98. H. Liu, Z. Lv, K. Ding, X. Liu, L. Yuan, H. Chen and X. Li, *J. Mater. Chem. B*, 2013, **1**, 5550-5556.
99. Z. Huang, D. Zhao, X. Deng, J. Zhang, Y. Zhang and X. Yu, *Nanomaterials*, 2018, **8**, 115.
100. S. Dinda, M. Ghosh and P. K. Das, *Langmuir*, 2016, **32**, 6701-6712.
101. X. Wu, Y. Li, C. Lin, X. Hu and L. Wang, *Chem. Commun.*, 2015, **51**, 6832-6835.
102. K. Liu, M. Abass, Q. Zou and X. Yan, *Green Energy Environ.*, 2017, **2**, 58-63.